

**UNIVERSIDAD DE INVESTIGACIÓN DE
TECNOLOGÍA EXPERIMENTAL YACHAY**

Escuela de Ciencias Químicas e Ingeniería

**TÍTULO: Effect of husk rice SiO₂ on the thermal and
mechanical properties of PLLA/PEG/SiO₂ composites**

Trabajo de integración curricular presentado como requisito
para la obtención del título de Ingeniero (a) de Polímeros

Autora:

Morales Carrera Johanna Belen

Tutora:

Ph.D. Alicia Sommer

Co-tutor:

Ph.D. Rodrigue Denis

Ingeniera de Polímeros – **Johanna Morales**

Urcuquí, diciembre 2022

AUTORÍA

Yo, **Johanna Belen Morales Carrera**, con cédula de identidad 1722690623, declaro que las ideas, juicios, valoraciones, interpretaciones, consultas bibliográficas, definiciones y conceptualizaciones expuestas en el presente trabajo; así como, los procedimientos y herramientas utilizadas en la investigación, son de absoluta responsabilidad de el/la autora (a) del trabajo de integración curricular. Así mismo, me acojo a los reglamentos internos de la Universidad de Investigación de Tecnología Experimental Yachay.

Urququí, diciembre 2022.



Johanna Belen Morales Carrera

CI: 1722690623

AUTORIZACIÓN DE PUBLICACIÓN

Yo, **Johanna Belen Morales Carrera**, con cédula de identidad 1722690623, cedo a la Universidad de Investigación de Tecnología Experimental Yachay, los derechos de publicación de la presente obra, sin que deba haber un reconocimiento económico por este concepto. Declaro además que el texto del presente trabajo de titulación no podrá ser cedido a ninguna empresa editorial para su publicación u otros fines, sin contar previamente con la autorización escrita de la Universidad.

Asimismo, autorizo a la Universidad que realice la digitalización y publicación de este trabajo de integración curricular en el repositorio virtual, de conformidad a lo dispuesto en el Art. 144 de la Ley Orgánica de Educación Superior.

Urcuquí, diciembre 2022.



Johanna Belen Morales Carrera

CI: 1722690623

Dedication

To my beloved family.

Acknowledgments

I would like to express my gratitude to my parents, who have supported me throughout my life and encouraged me to pursue my ambitions. To my siblings, who have supported me throughout my personal and professional development and have witnessed my growth firsthand. Bryan, for being my partner and accomplice and aiding me in achieving my objectives. Since this would not have been possible without the financial assistance of the "Emerging Leaders in the Americas Program (ELAP) Scholarship", I would like to thank the Government of Canada in particular. I am grateful to my Ph.D. professor, Alicia Sommer, for her advice, direction, teachings, and support. I give my Ph.D. thesis advisor thank Rose Mary Michell for her constant guidance and encouragement throughout this work and her insights, advice, and words of support. In addition, I want to thank Denis Rodrigue, my Ph.D. thesis co-supervisor, for his unwavering assistance in developing and characterizing the samples used in this research. I value his lectures, constant advice, willingness to collaborate with me, and exceptional investigative skills. Finally, thanks to Ph.D. Edward Avila for X-ray Diffraction patterns used in the present study.

RESUMEN:

Este estudio investigó el efecto del SiO₂ obtenida la de cáscara de arroz en la preparación de compositos de ácido poli-L-láctico/SiO₂ (PLLA/SiO₂) y ácido poli-L-láctico/SiO₂/polietilenglicol (PLLA/SiO₂/PEG) por el método de extrusión por fusión. Para los compuestos de PLLA/SiO₂, el SiO₂ se obtuvo de la incineración de cáscara de arroz y se mezcló con PLLA en varias concentraciones (5, 10 y 15 % en peso). Al mismo tiempo, los compuestos PLLA/SiO₂/PEG utilizaron PEG con un peso molecular de 6000 g/mol con varias concentraciones (0, 3, 5, 10 % en peso) y 10 % en peso de SiO₂. La morfología de la muestra se estudió empleando microscopía electrónica de barrido (SEM) para analizar la superficie y la miscibilidad del PEG en PLLA y la dispersión de SiO₂ en la matriz polimérica. Se desarrollo un estudio de calorimetría diferencial de barrido (DSC) para realizar un análisis no isotérmico e isotérmico de todas las muestras. La estabilidad térmica de los compositos se estudió mediante análisis termogravimétrico (TGA). Se utilizó el análisis de reología de fusión para investigar el comportamiento viscoelástico de los compositos. Las propiedades mecánicas de los compuestos se realizaron a temperatura ambiente utilizando una máquina universal Instron 5565 y el software Blue Hill. Para corroborar los resultados de cristalización obtenidos mediante DSC, se realizo análisis de difracción de rayos X (XRD). Finalmente, se desarrollaron las medidas de permeabilidad de gases utilizando un método de presión variable (volumen constante) para analizar el comportamiento de permeabilidad de las muestras a CO₂, CH₄, O₂ y H₂. Los resultados finales demostraron que las partículas de SiO₂ reducen la movilidad de la cadena de PLLA, lo que ralentiza el proceso de cristalización, aumenta el módulo de Young, la estabilidad térmica y la viscosidad, y reduce su permeabilidad a los gases. Sin embargo, la adición de PEG a los compuestos hizo que su tasa de cristalización aumentara incluso más que la del PLLA puro (>40 %), aumentando su elongación a la rotura (>26 %) y aumentando la flexibilidad del polímero. Debido a la mejor dispersión de sílice en la matriz polimérica y al aumento de la movilidad de la cadena PLLA, la viscosidad del material y la permeabilidad a los gases (>50 %) mejoran con la adición de PEG.

Palabras clave: ácido poli-L-láctico, sílice de cáscara de arroz, polietilenglicol, cristalización de polímeros.

ABSTRACT:

This study investigated the effect of rice husk SiO₂ on the preparation of Poly(L-lactic acid)/SiO₂ (PLLA/SiO₂) and Poly(L-lactic acid)/SiO₂/Poly(ethylene glycol) (PLLA/SiO₂/PEG) composites by the melt extrusion method. SiO₂ was obtained from rice husk incineration and mixed with PLLA preparation involves the use of various concentrations (5,10, and 15 wt%). At the same time, PLLA/SiO₂/PEG composites used PEG with a molecular weight of 6000 g/mol with various concentrations (0, 3, 5, 10 wt%) and 10 wt% SiO₂. The sample morphology was studied by scanning electron microscopy (SEM) to analyze the surface morphology and miscibility of PEG in PLLA and the dispersion of SiO₂ in the polymer matrix. A differential scanning calorimetry (DSC) study was used for non-isothermal and isothermal analysis of all the samples. The composites' thermal stability was studied using thermogravimetric analysis (TGA). Melt rheology analysis was used to investigate the viscoelastic behavior of the composites. Mechanical properties of the composites were evaluated at room temperature using an Instron 5565 universal machine and Blue Hill software. In order to corroborate the results of crystallization obtained in DSC, X-ray diffraction analysis (XRD) was used. Finally, gas permeation measurements were carried out using a variable pressure (constant volume) method to analyze the permeability behavior of samples to CO₂, CH₄, O₂, and H₂. The final results demonstrated that SiO₂ particles reduce the chain mobility of PLLA, which slows the crystallization process, raises Young's modulus, thermal stability, and viscosity, and decrease its gas permeability. However, adding PEG to the composites caused their crystallization rate to rise even higher than pure PLLA (>40%), increasing its elongation at break (>26%) and increasing the polymer's flexibility. Due to improved silica dispersion in the polymeric matrix and increased PLLA chain mobility, the material's viscosity and gas permeability (>50%) improve with the addition of PEG.

Keywords: Poly(L-lactide acid), Rice Husk Silica, Poly(ethylene glycol), polymer crystallization.

INDEX

1. Introduction	1
2. Background	3
2.1 Poly(L-lactid acid) composites.....	3
2.2 Effect of silica from rice husk on Poly(L-lactic acid) matrix.....	4
2.3 Effect of Poly(ethylene glycol) on Poly(L-lactic acid) matrix.....	5
2.4 Melt-compounding process	6
2.5 Properties of composites.....	6
2.5.1 Isothermal crystallization.....	7
2.5.1.1 Hoffman Weeks extrapolation.....	7
2.5.1.2 Avrami's theory.....	7
2.5.1.3 Lauritzen and Hoffman's theory.....	7
2.5.2 Thermal stability.....	8
2.2.2.1 Friedman's method	8
3. Problem statement.....	10
4. Objectives.....	11
4.1 General objective	11
4.2 Specific objectives	11
5. Methodology	11
5.1 Materials	11
5.2 Experimental description	11
5.2.1 SiO ₂ Preparation.....	11
5.2.2 Preparation of composites.....	12
5.3 Morphology of the samples.....	12
5.4 Non-isothermal crystallization.....	13
5.5 Isothermal crystallization	13
5.6 Thermogravimetric analysis	14
5.7 Melt rheology	14
5.8 Tensile test	14
5.9 Surface rupture morphology	14
5.10 X-ray diffraction analysis	14
5.11 Gas permeation measurements	15
6. Results and discussion	15

6.1	Morphology of the samples.....	15
6.2	Non-isothermal crystallization	18
6.3	Equilibrium melting temperature determination	22
6.4	Isothermal crystallization.....	25
6.5	Thermogravimetric analysis	34
6.6	Melt rheology	36
6.7	Tensile test	38
6.8	Surface rupture morphology.....	40
6.9	X-ray diffraction analysis	42
6.10	Gas permeation measurements	44
7.	Conclusions	46
8.	References	48

1. Introduction

In the last decades, the use of conventional petroleum-derived plastics has been less attractive because of their environmental impact. As more nations and states are banning plastic shopping bags and single-use plastics, which are blamed for so-called "white pollution" (1), the use and demand for biodegradable polymers have increased worldwide. One of the alternatives for those commodity polymers is poly(lactic acid) (PLA). This polymer has advantages like biodegradability, compatibility, and semicrystalline structure (2–4). This biodegradable polymer is made of renewable sources. It is produced mostly by the fermentation of simple sugars like glucose, maltose, and dextrose from corn and potato starch, sucrose from cane, and lactose from cheese whey (5–7). PLA has gained attention as a promising environmentally friendly packaging application reducing the use of petroleum-based commodity polymers (8,9). Due to the asymmetric carbon atom in lactic acid, a "set" of polymers with a specific number of stereo-sequences in the polymer macrochains can be produced by the sequential polymerization of optically active kinds of lactide (ll-lactide, dd-lactide, or meso ld-lactide). Commercial grades, frequently referred to as simply "PLAs," typically include an L-rich mixture since most of the bacteria employed in fermentation produce lactic acid primarily in the l-form with just a minor amount of D-LA impurities denominated PLLA (10). However, PLA has a variety of limitations that restrict its application in particular industries. PLA is a brittle polymer with slow rate crystallization, poor mechanical and permeability properties, and moderate degradation. Numerous processes are used to improve PLA's characteristics, including copolymerization (11,12), polymer compositing (13,14), polymer blending (15,16), plasticization (13,15–17).

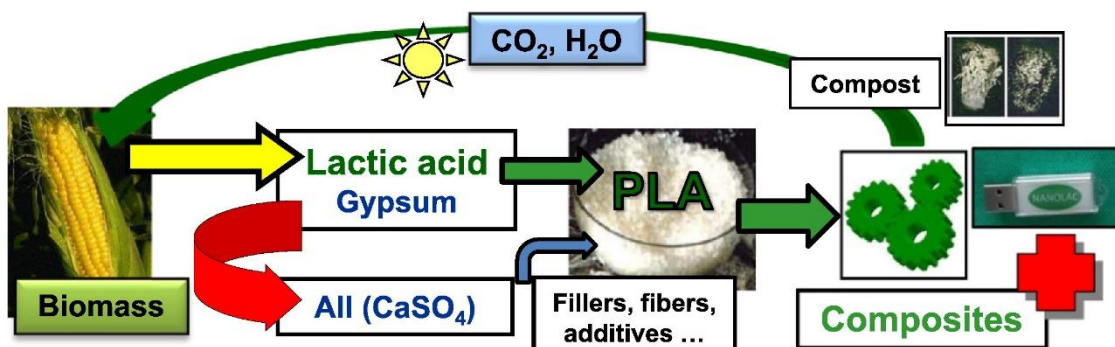


Figure 1. PLA composites: From production to properties (18).

Poly(ethylene) glycol (PEG), a biocompatible and flexible polymer, is an excellent choice for physically modifying the toughness of PLA (19). Because the terminal hydroxyl groups in PEG chains, it can react with the carboxyl groups in PLA molecules, PEG exhibits very strong miscibility with PLA (8). Jacobsen and Fritz (20) observed that adding PEG to PLA reduced both tensile strength and elasticity modulus, while increasing the percentage of elongation at the break. The addition of 10 wt% PEG increased impact resistance by approximately five times greater than pure PLA. However, it is essential to understand that the improvements that PEG can bring to the PLA have a limit. Sheth et al. (21) discovered that PLA/PEG mixes ranged from entirely miscible to moderately miscible depending on the PEG content. The composites obtained had higher elongation and lower modulus values when the PEG component was less than 50% by weight. However, beyond 50% PEG content, the composite morphology was altered by increasing PEG crystallinity, leading to a rise in modulus and a corresponding drop in elongation at the break. Due to the nature of PEG, when being mixed with PLA, the crystallinity of PLA increases, and cold crystallization temperatures, glass transition temperature, and melting temperature of PLA molecules decrease remarkably, as a consequence, increasing the crystallization rate (15).

Composites of bio-based polymers and fillers are one such increasingly sought material. Agricultural fillers can be used as reinforcement for PLA in composites because of their advantages: renewability, abundance, high specific strength, low density (22), cost efficiency, lightweight, and less environmental impact during production (23). One example of such agricultural filler is SiO₂ obtained from rice husk. After milling rice, rice husks are often dumped (24). Rice husks constitute more than 20% of the harvested grain with over 20% SiO₂ compositions (25). Research incorporating rice husk silica as reinforcement for agricultural filler-reinforced PLA composites has gained significant attention in the literature (10,14,26–31). Praprudivongs et al. (14) studied the biodegradation behavior of PLA. They crosslinked PLA filled with precipitated SiO₂ (commercial SiO₂) and SiO₂ from rice husk ash. They found that SiO₂ incorporation enhanced the degree of degradation. In particular, introducing commercial SiO₂ in PLA and crosslinked PLA tended to increase the degree and rate of biodegradation. According to Opaprakasit et al. (31), PLA/silica composites improve gas permeability and selectivity. They also determined that the materials had a strong potential for usage as degradable packaging films with adjustable gas permeability.

In the same way, Battegazzore et al. (26) discovered that the presence of extracted silica in 5/10/20 and 30 wt% resulted in significant increases in Young's modulus and a slight decrease in the oxygen permeability of PLA. Several studies on the effect of silica on the mechanical properties, permeability to water vapor and oxygen, and thermal degradation of PLA have been conducted to current days. The impact of silica addition to PLA/PEG composites has been studied. Aydın & Geyikçi (28) discovered that PLA/PEG/SiO₂ films had improved its thermal stability and water absorption/capture capacity with increased silica concentration. The silica from rice husk is known to act as a filler in the polymeric matrix. It provides several benefits to the final product. However, no comprehensive and comparative study of the effect of rice husk silica in PLA matrices and PEG in PLA/SiO₂ composites has been conducted.

Our study investigates the effect of the husk rice SiO₂ as a filler on the properties of PLLA/SiO₂ composites at various SiO₂ contents. As was previously reported in the literature, SiO₂ can improve permeability, Young's modulus, and thermal degradation of the PLLA. However, other properties, such as elongation at the break, rate crystallization, tensile strength, complex viscosity, and crystallization degree, are affected. An extensive evaluation of crystallization kinetic has been investigated to study the outcome of PLLA plasticization with PEG and SiO₂ particles for various applications. The rheology, mechanical, thermal stability, permeability, and morphological properties of PLLA/SiO₂ and PLLA/SiO₂/PEG composites were also studied.

2. Background

2.1 Poly(L-lactid acid) composites

PLA synthesis can occur either by condensation polymerization of the lactic acid monomer or by ring-opening polymerization of lactide, which is its cyclic dimer. The most recent method, ring-opening polymerization, creates PLLAs for common applications. Film and packaging, textile and fiber, construction, and automotive products are some of these uses (32).

As mentioned, PLA has several intriguing characteristics, including high tensile strength and rigidity, or high Young's modulus. However, it has some disadvantages, including low flexibility, ductility, impact resistance, and heat distortion temperature.

Also, a lengthy injection molding cycle time because of a slow crystallization rate, a high sensitivity to moisture, a low resistance to hydrolysis, and other issues (18).

In addition, PLA-based products with specific end-use properties are available, including those that increase crystallization speed by incorporating nanofillers (33), increase toughness and impact resistance by adding a flexible polymer (34), increase flame retardancy by adding talc (35), improve electrical conductivity by adding graphene (36), and improve anti-UV and antimicrobial properties by adding oxides (37), and more. The properties of the final product will depend on several factors, including the size of the particles, the manufacturing conditions, the amount of filler, the treatment of the particles, previous elaboration of the composites, etc.

2.2 Effect of silica from rice husk on Poly(L-lactic acid) matrix

Aydin and Geyikçi (28) found that due to the difficulty in removing volatile components from the structure and shifting the thermal breakdown temperature to higher temperatures, silica-doped PLA has better thermal stability than pure PLA. The capacity to absorb water determines how quickly biodegradable polymers break down in a compost environment. In general, PLA can disintegrate fully after two years. Since the fillers' hygroscopic properties boosted their capacity to absorb water, silica-doped PLA can degrade more quickly than pure PLA. The water absorption capabilities of the silica-containing film increased from 9% to 21% as the filler concentration increased from 10% to 20%. According to Battezzore et al. (26), extracted silica caused PLA's Young modulus to improve noticeably while somewhat lowering its oxygen permeability. The mechanical properties obtained proved to be better than those displayed by comparable samples made using commercial silica. Huang et al.(38) successfully dispersed the SiO₂ particles in PLA at a filler content of 5 wt%. According to the TGA and DTA data, amino-silica could enhance the thermal and mechanical properties of PLA/SiO₂ composites. However, the DSC results shows that T_g appears unaffected by the loading of SiO₂ particles. PLA/silica composites with silica concentrations ranging from 0-2.0 wt% were prepared by Opaprakasit et al. (31). Improvements in gas permeability and selectivity were attained, most likely due to the creation of voids brought on by the silica particles' phase incompatibility with the PLA matrix. They concluded that the composites could be used to make degradable packaging films with adjustable gas permeability. Because silica

particles are made from bio-based resources, these composites retain their potential to biodegrade.

As a result, we can assume that the effects of rice husk silica on the PLLA polymeric matrix are: an increase in Young's modulus, an increase in rigidity, an increase in thermal stability due to the difficulty in removing the volatile components of the structure silica, a greater capacity for degradation due to the hygroscopic nature of silica, and a decrease in its permeability to oxygen, allowing its use as membranes in food packaging and other.

2.3 Effect of Poly(ethylene glycol) on Poly(L-lactic acid) matrix

Mohapatra et al. (39) argued that adding PEG to the PLA matrix increases the latter's ductility while lowering its tensile strength and tensile modulus. The blend's maximum impact strength increased 32 times over PLA when made at an 80:20 PLA: PEG ratio. According to DSC experiments, adding PEG to the PLA matrix reduces T_g and T_c . This is mostly because of the PEG's plasticizing impact. The thermal deterioration of PLA is facilitated by the addition of PEG, which lowers PLA's thermal stability, according to the TGA of the sample performed in nitrogen. The modulus of blends with less than 30 wt% PEG content drops, and the strain increases as the PEG level rises. However, the crystallization of the PEG component causes the blends' modulus to increase and their elongation at break to drastically fall over 30 weight percent. Wang et al. (40) found that the tensile characteristics show that the PEG addition improves the segmental mobility of PLA chains and increases PLA's capacity for plastic deformation, lowering yield stress and raising elongation at break. In their study of the tensile properties of PLA at different PEG molecular weights (6000, 10000, and 20000 g/mol), Li et al. (41) found that adding the right amount of lower molecular weight PEG could more effectively increase PLA's tensile toughness. The PEG's improved compatibility explained this with PLA and the increased mobility of the PLA molecular chains. While stretching, a significant amount of crazing needed to occur on the PLA/PEG surfaces, which required substantial energy consumption and improved tensile toughness. Additionally, the simple and practical blend modification process broadens the range of applications for PLA, and the generated blends can be used to make biocompatible/bioabsorbable medical devices and food packaging.

In conclusion, PEG is an effective plasticizer for PLA because it increases the chain's mobility, changes thermal properties by enhancing the crystallization rate, and enhances mechanical qualities like elongation at break.

2.4 Melt-extrusion process

After being developed in the early 1930s, the hot melt extrusion method has quickly emerged as the most used processing technique in the food, rubber, and plastics manufacturing sectors. Hot melt extrusion involves several compression stages that result in a uniformly dense and shaped end product from the powdered materials. When PLA is used in a hot melt extrusion process, the revolving screws propel the PLA and active ingredients, together with any additives like silica particles and PEG, in the direction of the die while maintaining precise control over the temperature, pressure, feeding rate, and screw speed (42).

The processing of PLA makes it highly susceptible to heat and hydrolytic degradation. To minimize early degradation, PLA must be processed under the mildest circumstances possible while producing the appropriate qualities. Melt processing conditions are typically characterized by high temperature and shear. Thus, there is a need to determine the optimum processing conditions to achieve the desired properties of extruded PLA (43). The T_m of PLA is roughly 170 °C (44), in practice, PLA is melted at a temperature of 230 °C. As a result, the maximum extrusion temperatures were set to 200 and 250 °C, for thermocouples.

2.5 Properties of composites

Determining the crystallization kinetic parameters, such as the spherulite growth rate and overall crystallization, using the isothermal crystallization experiment is useful to describe the effect of different fillers on the PLA matrix (45). The isothermal crystallization result is very sensitive to the sample properties. The average molecular weight, molecular weight distribution, type and concentration of the filler, the concentration of that filler, the presence of plasticizers, or the presence of regrind are just a few of the variables that can affect isothermal crystallization. As a result, it is a sensitive test that can be used to distinguish between different batches of material that might not stand out in a standard heating experiment. The final processed product's quality will vary depending on the crystallization behavior of different batches (46).

2.5.1 Isothermal Crystallization

2.5.1.1 Hoffman-Weeks extrapolation

T_m^0 is generally estimated by linear extrapolation of the T_m versus T_c plot to the line $T_m = T_c$, as expressed by linear Hoffman–Weeks (HW) extrapolation

$$T_m = \frac{T_c}{\gamma} + T_m^0 \left(1 - \frac{1}{\gamma}\right) \quad (1)$$

where γ is the thickening ratio (4).

2.5.1.2 Avrami's Theory

Avrami's theory is often used to model isothermal crystallization kinetics using overall crystallization rate data. In this work, we followed the experimental protocols and analyses established previously by Lorenzo et al. (47,48) to minimize issues associated with using the Avrami equation to investigate DSC isothermal crystallization kinetics. The Avrami equation can be expressed as:

$$1 - V_c(t) = \exp(-kt^n) \quad (2)$$

Where: V_c is the relative volumetric transformed fraction, n the Avrami index, and k is the overall crystallization rate constant containing contributions from nucleation and growth (47) (49). Parameters n and k can be obtained from the slope and intercept of the Avrami plot of $\log[-\ln(1 - X_t)]$ vs $\log(t)$ according to Lorenzo et al. (47).

The conversion range is usually from 3 to 20%, which corresponds to the primary crystallization range; this range can be varied for more precision above 0.9990 for R^2 to indicate an excellent fit of the data in a specific conversion range (47).

2.5.1.3 Lauritzen Hoffman's Theory

Hoffman evaluated experimental data on spherulite growth rate using the secondary nucleation theory. The Hoffman and Lauritzen equation (50) is given by:

$$G = G_0 \exp\left(-\frac{U^*}{R(T_c - T_\infty)}\right) \exp\left(-\frac{K_g}{T_c \Delta T f}\right) \quad (3)$$

Where ΔT is the degree of supercooling defined by $T_m^0 - T_c$; T_m^0 is the equilibrium melting point which is 480 K (51,52); T_c is crystallization temperature; f is a factor

expressed as $\left(\frac{2T_c}{T_m^0 + T_c}\right)$; U^* the activation energy for segment diffusion to the crystallization site was used 1500 cal/mol (6276 J/mol) in order to compare the results with the literature; R is the gas constant; T_∞ is the hypothetical temperature expressed as $(T_g - 30 \text{ K})$, T_g determined by DSC, G_0 is the front factor and K_g is the nucleation constant and is defined as:

$$K_g = \left(\frac{Zb_0\sigma\sigma_e T_m^0}{\Delta h_f k_B} \right) \quad (4)$$

where σ is the lateral surface free energy, σ_e is the fold surface energy, b_0 is the layer thickness of the crystal, Δh_f is the volumetric heat of fusion, and k_B is the Boltzmann constant (49). The value of Z is dependent on the crystallization regime and equal to 4 for Regimes I and III and values 2 for Regime II (53). For neat PLLA, the value of σ_e is $97 \times 10^{-3} \text{ J/m}^2$ which is in the range of values reported in the literature $43.5 \times 10^{-3} \text{ J/m}^2$ by (54) and $107 \times 10^{-3} \text{ J/m}^2$ by (51) (55). It has been demonstrated that the value of σ_e is affected by the molecular weight of PLLA (51) and the cooling or heating rate of the isothermal crystallization temperature (54,55).

Chain folding, q , is connected with molecular structure and involves bending the polymer chain back onto itself in the suitable form. Chain folding can be expressed as (56):

$$q = 2a_0b_0\sigma_e \quad (5)$$

2.5.2 Thermal Stability

2.5.2.1 Friedman's method

The E_a of polymers has primarily been determined through kinetic studies as a function of conversion rate without any prior assumption of the kinetic model using isoconversional (model-free) approaches. One of the isoconversional methods used to determine the precise value of the E_a at a specific conversion rate is the Friedman approach. The Friedman method followed the differential procedure for calculating E_a , $\ln(A)$, n , R^2 .

Friedman's method provides accurate E_a at a given conversion rate; even E_a is a function of conversion rate. The E_a is determined from the slope of a straight line plot

against $1/T$ obtained from TGA curves. For the thermosetting resins, the rate of conversion (da/dt) is usually expressed as:

$$\ln \frac{d\alpha}{dt} = A * \ln f(\alpha) - \frac{E_a}{RT} \quad (6)$$

where A and E_a are kinetic parameters, the pre-exponential factor and the activation energy, respectively, R is the universal gas constant, and T is the absolute temperature at time t. α is the fractional extent conversion at a given time (or given temperature), expressed as:

$$\alpha = \frac{m_i - m_t}{m_i - m_f} \quad (7)$$

where m_i is the mass of samples before thermal degradation, m_t is the mass of samples at time t during thermal degradation, and m_f is the mass of samples after thermal degradation (also called char yield) (57).

3. Problem Statement

Several nations have banned plastic bags, straws, plates, cups, disposable cutlery, and other single-use plastics due to rules that have become more prevalent in recent years regarding their use. Because of this, both businesses and customers choose biodegradable products like biopolymers. One of the most researched and often used biopolymers is polylactic acid. However, it has numerous drawbacks, including a low crystallization rate, subpar mechanical characteristics, and non-selective permeability. Therefore, adding SiO_2 as a filler and PEG as a plasticizer to PLA is suggested to increase its quality.

4. Objectives

4.1 General Objective

To improve the thermal, mechanical, rheological, and permeable properties of polylactic acid by adding SiO₂ as filler and PEG as a plasticizer.

4.2 Specific Objectives

1. To extract high-purity SiO₂ from rice husks through acid treatment and subsequent incineration.
2. To prepare PLLA composites with different SiO₂ concentrations.
3. To prepare PLLA composites with a given amount of SiO₂ and different PEG concentrations.
4. To characterize composites to describe their behavior with SiO₂ as filler and PEG as a plasticizer.

5. Methodology

5.1 Materials

Rice husk has provided by Université Laval Quebec, Canada. PLLA 4043D with 94% l-lactide and 6% d-lactide content was purchased from Ingeo Nature Works, and PEG for synthesis with a molecular weight $M_w = 6000$ g/mol was purchased from Merck Millipore.

5.2 Experimental Description

5.2.1 SiO₂ Preparation

Rice husk was ground with an industrial mill and then washed with a solution of HCl 1M for two hours. After that, the rice husk was washed with distilled water ten times until the pH solution was neutral. Then, the rice husk was left in the oven at 60 °C overnight. Once the rice husk was dry, it was placed at 600 °C for 7 hours to obtain amorphous SiO₂.

5.2.2 Preparation of Composites

Grounded PLLA and SiO₂ were predried for two hours at 60 °C to remove moisture content present in the material. Mixing of PLLA, PEG, and SiO₂ at different concentrations were melt-blended by using a co-rotating twin-screw extruder (Leistritz ZSE-27, Nürnberg, Germany) with an L/D ratio of 40 and 10 heating zones (die diameter of 2.7 mm). The total flow rate was 0.5 kg/h, and the screw speed was adjusted to 70 rpm and the side feeder to 50 rpm. Because PLLA exhibits the maximum melting temperature between 175 and 180 °C (58), the temperature profile was chosen at 175 °C for the first zone, 190 °C for the second to the eighth zone, 170 °C for the ninth zone and 150 °C to the tenth zone to limit degradation. All the different concentrations of PLLA/PEG/SiO₂ were fed to the extruder through the first zone (main feeder). After cooling in a water bath, the mixes were pelletized using a model 304 pelletizer (Conair, CA, USA), then dried at 60 °C for 2 hours to remove any remaining water.

Table 1. Formulations for the PLLA/SiO₂ and PLLA/SiO₂/PEG composites

Sample	PLLA (wt%)	SiO ₂ (wt%)	PEG6000 (wt%)
PLLA	100	-	-
PLLA/SiO ₂ (95/5)	95	5	-
PLLA/SiO ₂ (90/10)	90	10	-
PLLA/SiO ₂ (85/15)	85	15	-
PLLA/SiO ₂ /PEG (90/10/3)	90	10	3
PLLA/SiO ₂ /PEG (90/10/5)	90	10	5
PLLA/SiO ₂ /PEG (90/10/8)	90	10	8
PLLA/SiO ₂ /PEG (90/10/10)	90	10	10

5.3 Morphology

An Inspect F50 scanning electron microscope (SEM) (FEI, Hillsboro, OR, USA) was used at 10 kV to take the SiO₂ from the rice husk and 5-10 kV to take micrographs of cryogenic cut and the fracture surface of the PLLA and PLLA composites.

Energy dispersive spectroscopy (EDS) was used to study SiO₂ from rice husk and identify contaminants using the same equipment.

5.4 Non-isothermal crystallization

A PerkinElmer Pyris DSC-8 differential scanning calorimeter connected to a cooling system and calibrated with pure indium and tin standards, was used. Samples of approximately 5 mg, sealed in aluminum pans, were used, and all experiments were performed under N₂ atmosphere with a flow of 20 mL/min.

For the non-isothermal cold crystallization, the samples were melted at 200 °C, then to erase the thermal history the samples were holding at that temperature for 3 min, and cooled from the melt at 10 °C/min to 0 °C. After equilibration, the samples were heated to 200 °C with heating rates 10 °C/ min.

The degree of crystallinity (X_c) of the neat PLLA and PLLA composites was calculated using the equation:

$$X_c(\%) = \left(\frac{\Delta H_m - \Delta H_{cc}}{\Delta H_m^0} \right) \cdot \left(\frac{1}{w} \right) \cdot 100\% \quad (8)$$

where ΔH_m is the experimental heat of fusion determined from DSC, ΔH_m^0 is the theoretical heat of fusion of the 100% crystalline PLLA (93 J/g), ΔH_{cc} is the cold crystallization enthalpy and w is the weight fraction of PLLA in the composites.

5.5 Isothermal Crystallization

After erasing the thermal history for 3 minutes at 200 °C, the samples were cooled from the melt to 0 °C at an average rate of 80 °C/min to prevent crystallization during cooling. The sample was then heated to the desired crystallization temperature. The exotherm crystallization is recorded as a function of time until saturation was attained (about three times the half-crystallization duration). The sample was then heated at a rate of 20 °C/min to record the melting behavior of the isothermally crystallized composite. Previous tests were performed to identify the appropriate crystallization temperatures (T_c). The sample was cooled from the melt at 80 °C/min to a predetermined T_c and then heated at 20 °C/min to test whether any melting could be observed. Then a test with a more excellent T_c was done until no crystallization occurred during the preceding cooling. A T_c temperature range of at least six different temperatures was used (47).

5.6 Equilibrium melting temperature determination

The Hoffman-Weeks (HW) method involves the extrapolation of a linear regression of experimentally observed melting temperatures, T_m , for various crystallization temperatures, T_c , to the equilibrium line $T_m = T_c$. After isothermal crystallization, the samples were heated to 200 °C. For our samples, we obtained two melting peaks. T_m^0 was calculated by extrapolating the first fusion peak to where $T_m = T_c$ intersected.

5.7 Thermogravimetric Analysis

The weight curves obtained by TGA were recorded using a TA Instruments model Q5000IR from 30 to 600 °C at a heating rate of 10 °C/min under nitrogen atmosphere.

5.8 Melt Rheology

An ARES (TA Instruments, New Castle, DE, USA) rotational rheometer with 25 mm discs and 3 mm gap was used to characterize the viscoelastic properties in the melt state. All of the experiments were carried out at 190 °C under a nitrogen atmosphere. After performing dynamic strain sweeps to determine the limits of the linear viscoelastic range, frequency sweeps were performed at a strain of 0.01 to 100%. From the data obtained, the elastic modulus, complex viscosity, storage modulus and damping factor ($\tan(\delta)$) were analyzed to quantify the rheological properties in the melt state.

5.9 Tensile Test

Tensile tests were performed at room temperature using an Instron 5565 universal machine and Blue Hill software examined at 2 mm/min. The average value was calculated after five samples were tested.

5.10 Surface rupture morphology

An Inspect F50 scanning electron microscope (SEM) (FEI, Hillsboro, OR, USA) was used at 10 kV to take the SiO₂ from the rice husk and 2-5 kV to take micrographs of the tensile test rupture surface.

5.11 X-ray Diffraction Analysis

X-Ray Diffractometer Rigaku, with a voltage of 30 kV and current of 20mA was used to obtain the patterns of the PLLA composites. Before carrying out the

measurements, the samples were subjected to the following heat treatment. The samples were prepared in the sample holders and then heated for one hour at 80 °C in a vacuum oven.

5.12 Gas Permeation Measurements

The membranes were tested for pure gases N₂, O₂, CO₂, and CH₄. The pure gas transport properties were measured using a variable pressure (constant volume) method (59). For pure gases, the permeability coefficient P (cm³ cm/cm² s cmHg) was calculated as follows:

$$P = \frac{22.414}{A} \cdot \frac{V}{RT} \cdot \frac{l}{\Delta p} \cdot \frac{dp}{dt} \quad (9)$$

where A is the membrane area (cm²); l is the membrane thickness (cm); Δp is the upstream pressure (psi); V is the downstream volume (cm³); R is the universal gas constant (6236.56 cm³ cmHg/mol K); T is the absolute temperature (K), and dp/dt is the permeation rate (psi/s). The permeabilities are reported with units of Barrer (10⁻¹⁰ cm³ (STP) cm/ (cm² s cmHg)).

The permeation measurements were performed at the same temperature (35 °C) and same feed pressure (40 lb/in²).

6. Results and Discussion

6.1 Morphology

Studying the morphology of the composites is important to examine the interaction between the polymeric matrix and the filler, and the miscibility of PEG in the polymeric matrix. Also, PLA's physical, mechanical, and barrier properties are affected by its morphology (60). As shown in Figure 2.1, the obtained EDS spectrum depicts peaks corresponding to silicon and oxygen, indicating that the particles obtained are mostly SiO₂. There are traces of Au and Pd in low quantities due to the soil's chemical products or contaminants. These findings confirm the presence of the expected elements, indicating that silica was successfully extracted.

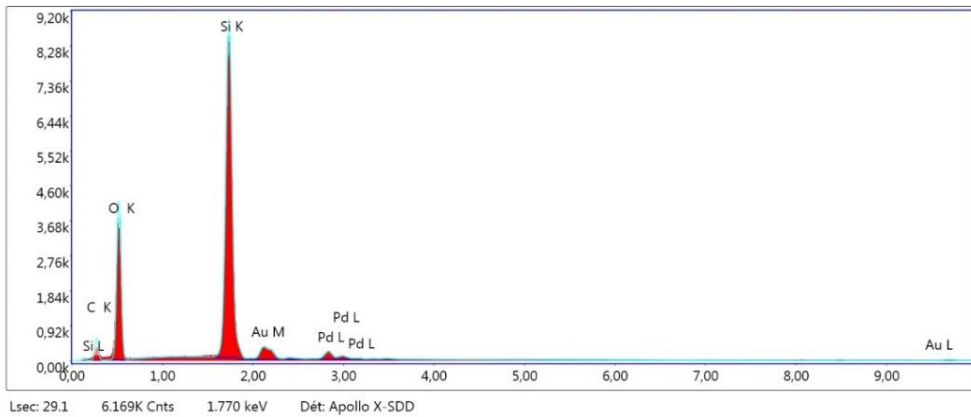
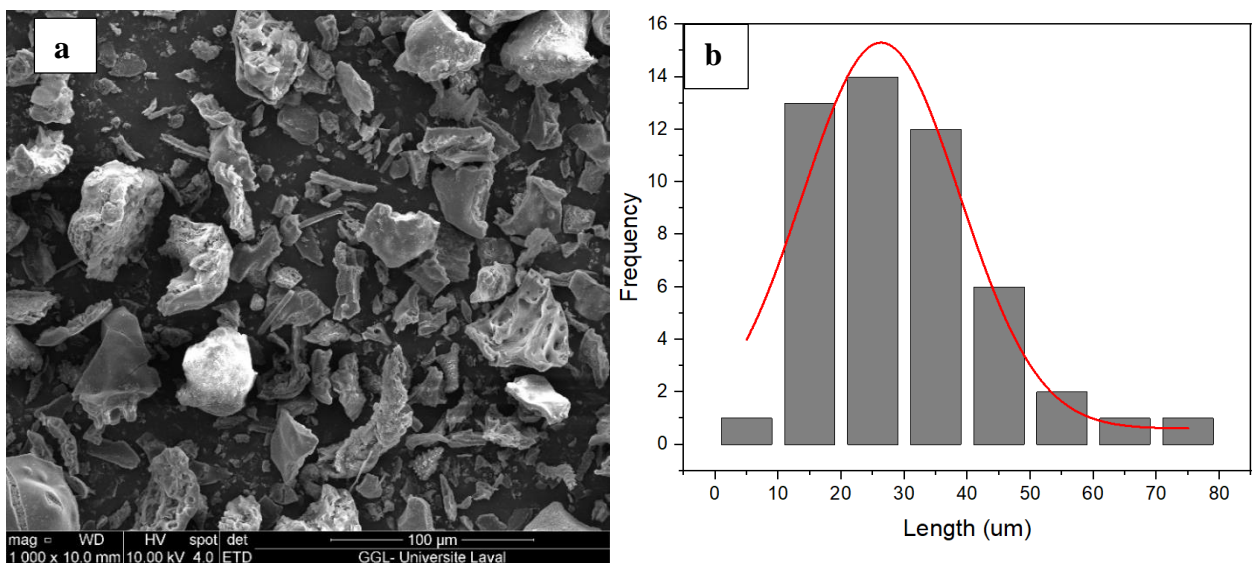
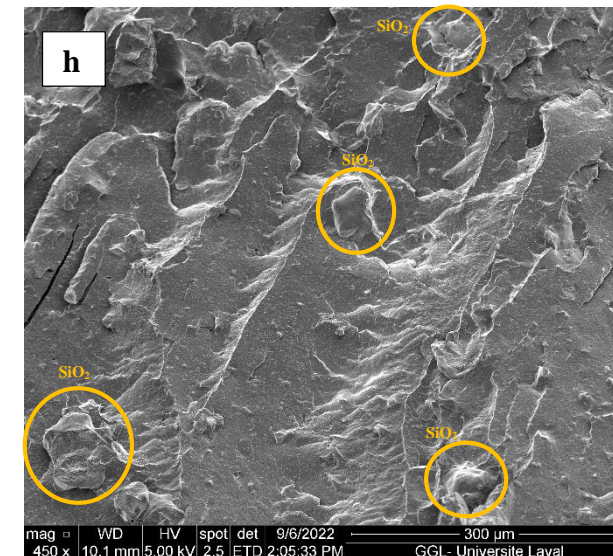
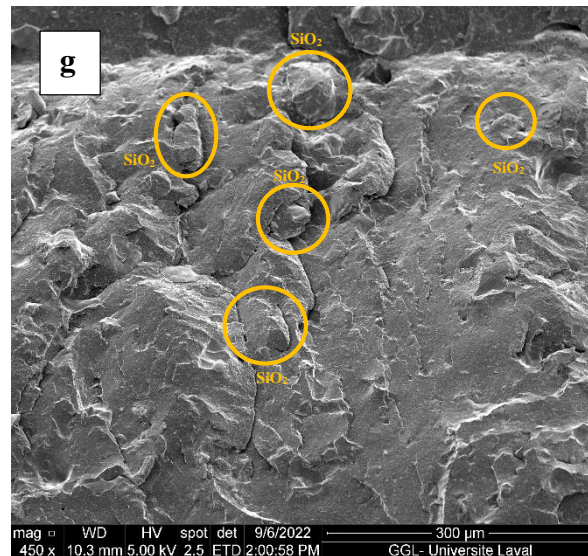
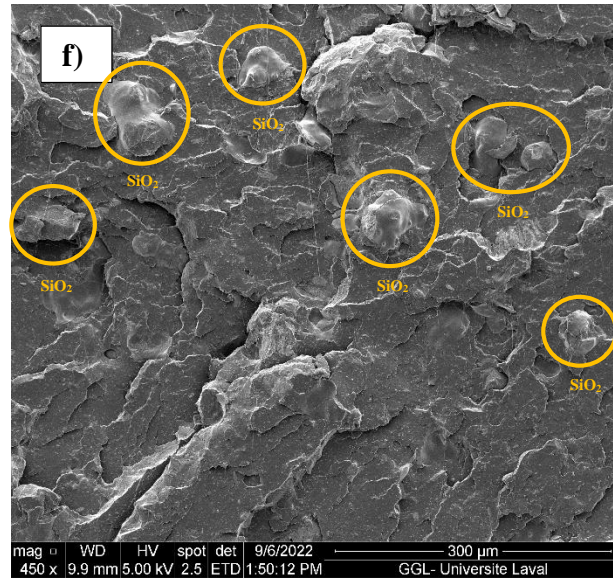
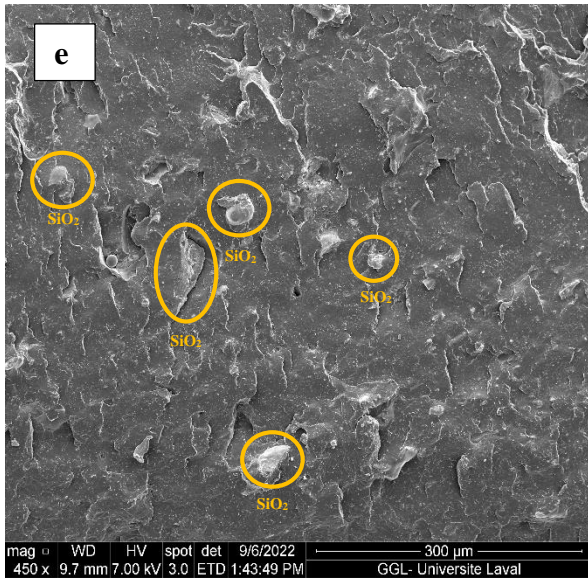
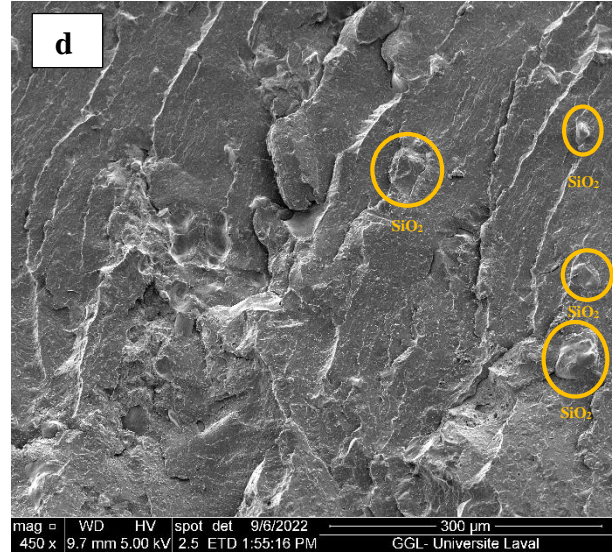
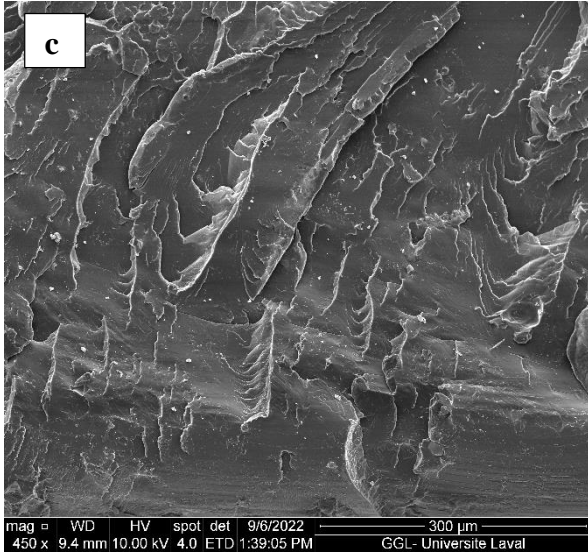


Figure 2.1 EDS spectra of the SiO₂ particles showing the purity of the sample.

Figure 2.2 (a) shows a micrograph of SiO₂ extracted from rice husk showing amorphous particles of different sizes and shapes. Figure 2.2 (b) shows its size distribution represented in a histogram, which ranges from 10 to 40 micrometers, as depicted. Figure 2.2 (c) demonstrates that pure PLLA has a homogenous surface with a brittle fracture, highlighting the material's fragility (61). The SiO₂ is distributed uniformly throughout the PLLA/SiO₂ composites, as is shown in Figures 2.1 (d-f), indicating a strong interaction between the two materials, as seen by the absence of cavities in the matrix and decohesion of the particles. Figures 2.2 (g-j) depict the surface of the PEG-based composites; compared to PLLA/SiO₂ composites, the samples exhibit a smoother surface and a superior silica particle distribution. Because both PLLA and PEG contain significant amounts of hydroxyl groups, it can be shown that they are compatible with one another (62).





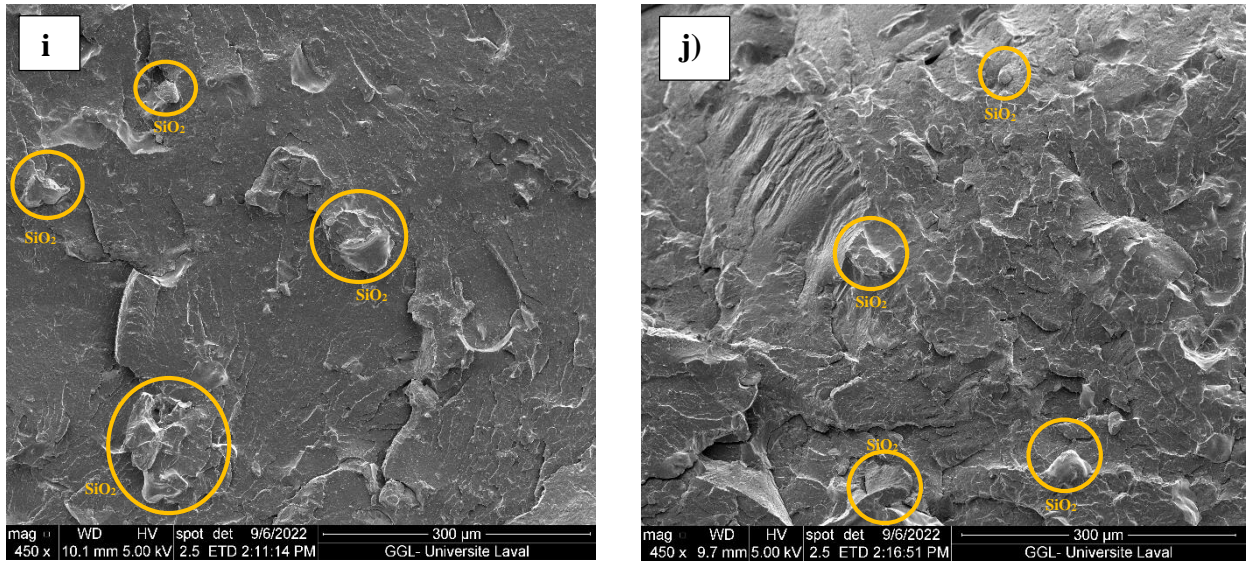


Figure 2.2. SEM micrograph of SiO₂ from rice husk (a), SiO₂ particle size histogram (b), pure PLLA (c), PLLA/SiO₂ (95/5) (d), PLLA/SiO₂ (90/10) (e), PLLA/SiO₂ (85/15) (f), PLLA/SiO₂/PEG (90/10/3) (g), PLLA/SiO₂/PEG (90/10/5) (h), PLLA/SiO₂/PEG (90/10/8) (i), PLLA/SiO₂/PEG (90/10/10) (j).

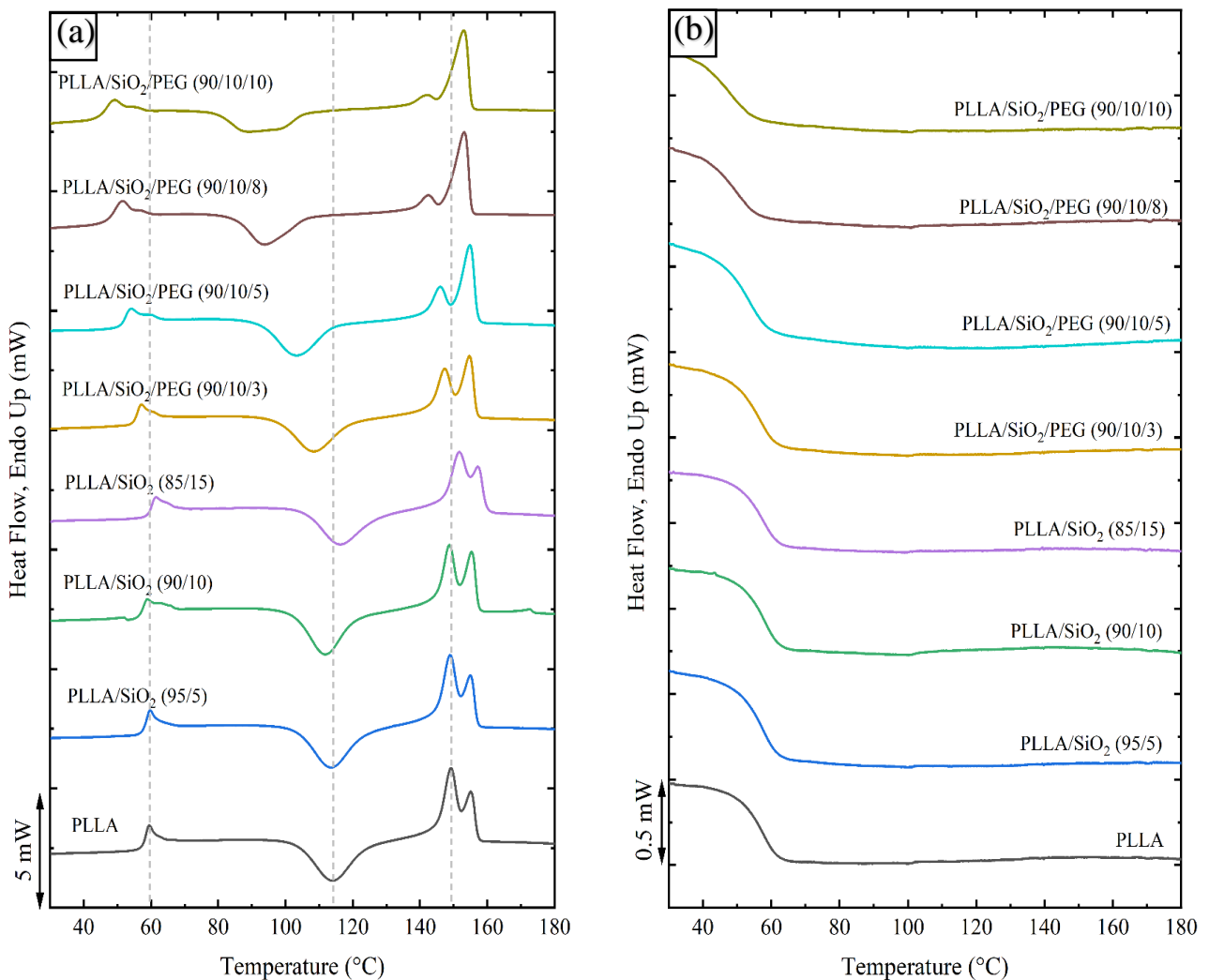
6.2 Non Isothermal Crystallization

Since learning about the effect of the SiO₂ particles on the ordering arrangement of PLLA chains was the primary goal of adding into PLLA matrix, the analysis is concentrated on the crystallization process of the composites. The DSC thermograms for first heating and cooling of the composites are presented as Figure 3 (a) and (b), respectively. Figure 3 (a) presents a slight decrease in glass transition temperature (T_g) and cold crystallization temperature (T_{cc}) for composites with 5 and 10% of silica, due to the previous crystallization temperature of the composites in the samples fabrication. Also, no change in T_m is observed since, for the first and second heating, it is observed at approximately 150 °C. The two expected polyester melting peaks are observed, and the changes in peaks melting temperature are explained in the second heating analysis. Figure 3 (b) shows no crystallization peaks; only the glass transition temperature at approximately 60 °C.

The second heating thermograms are displayed in Figure 3 (c) for samples containing 0, 5, and 10 wt% of silica. The glass transition (T_g) appeared at approximately 60 °C, indicating that the inclusion of silica did not appear to significantly impact its position at those concentrations. Cold crystallization behavior is typical for aliphatic polyesters such as PLA. It reflects the material's ability to crystallize below the melting temperature (63). Because crystallization occurs during the heating scan, an increase in T_{cc} in PLLA/SiO₂ (85/15) indicates a difficulty in the crystallization process, decreasing mobility and free volume. Then, an increase in T_{cc} could be attributed to the high concentration of silica in the PLLA matrix that hinders crystallization (64). Since this exothermic event concluded, a melting process occurred. It was distinguished by the occurrence of two melting peaks. According to the melt-recrystallization model, the melt-recrystallization mechanism causes unstable, tiny crystals to become more stable over time. In other words, the heating process creates competition between melting and recrystallization. This model states that the exothermic peak occurs when the rate of recrystallization exceeds the rate of melting, and the endothermic peak occurs when the rate of melting overwhelms recrystallization (4,65,66). This lower temperature peak also could be related to the melting of α' -crystals and their recrystallization into the α -crystalline form, whereas the higher temperature peak corresponds to the melting of the α form. The α' and α crystalline phases transition can be defined as melting the α' form and recrystallization into the α form (67). Silica in high concentrations caused recrystallization to be challenging due to a loss in chain mobility, as seen by the appearance of a single fusion peak for the compound with the highest silica concentration.

In order to increase silica particle dispersion in the PLLA matrix, different amounts of PEG were added to evaluate the crystallization rate and the interaction with PLLA/SiO₂ system. T_g is an excellent indicator of polymer structure and chain mobility (68). The decrease in T_g as a function of plasticizer concentration was used to assess plasticizing efficiency. The observed values of the glass transition, transition temperatures, the corresponding enthalpy values, and crystallinity percentage (X_c) of second heating for each composition are summarized in Table 2. As shown in Figure 3 (c), the T_g signal decreases with increasing PEG content compared to PLLA; it decreases from 59.9 °C to 49.6 °C (Table 2), showing good miscibility between the polymeric matrix and the plasticizer (69). Due to an increase in molecular mobility, the possible

migration of the plasticizer towards the PLLA matrix may be a component that affects the decrease in T_g (70). The T_{cc} and T_g decreased as the PEG percentage increased, which is consistent with the notion that PLLA crystallizes more easily at lower temperatures due to increased chain mobility (68) and chain-packing (71) occurred easily as the plasticizer amount increased. The rise in crystallinity of the compounds with PEG is another point to note. By increasing the PEG content, the percentage of crystallinity rises to 90% compared to pure PLLA and up to 40% compared with the composite with 10 wt% silica. This increase is because PEG simplifies the process for the polymer chains to be ordered and aligned (70).



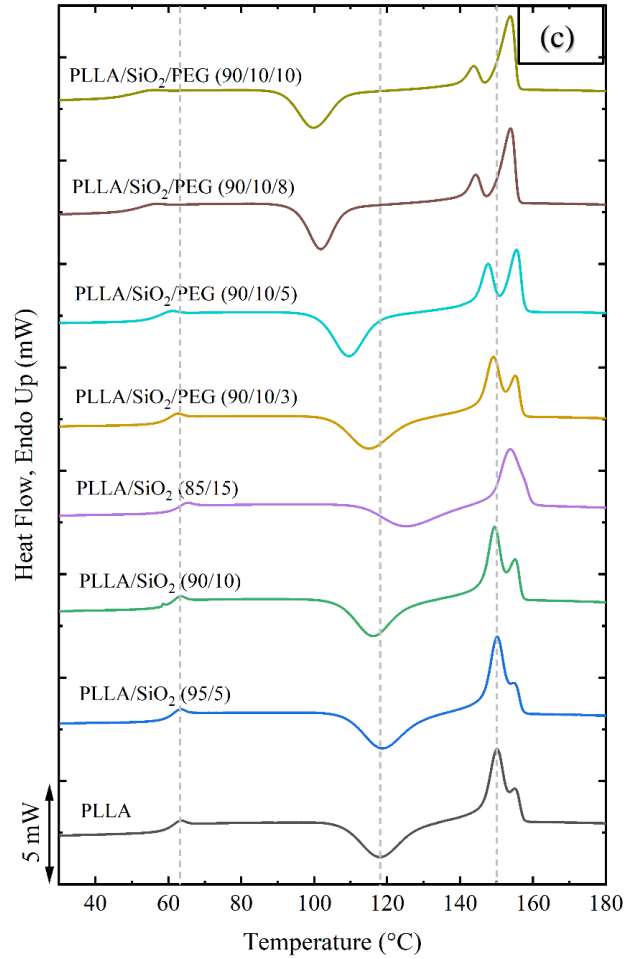


Figure 3. Thermogram of a) first heating, b) cooling, and second heating c) of the DSC scan of the PLLA, PLLA/SiO₂, and PLLA/SiO₂/PEG composites.

Table 2. Enthalpy of fusion, glass transition, melting temperature and degree of crystallinity of PLLA composites during the second heating at 10 °C/min.

Sample	2 nd Heating					
	T _{cc} (°C)	ΔH _{cc} (J/g)	T _g (°C)	T _m (°C)	ΔH _m (J/g)	X _c (%)
PLLA	118.0	-23.8	59.9	150.1 / 155.1	26.9	3.4
PLLA/SiO ₂ (95/5)	118.7	-25.2	59.9	150.2 / 155.0	27.2	2.3
PLLA/SiO ₂ (90/10)	116.1	-22.5	59.9	149.5 / 155.1	26.4	4.6
PLLA/SiO ₂ (85/15)	125.2	-17.6	61.8	153.8	21.3	4.7
PLLA/SiO ₂ /PEG (90/10/3)	115.0	-23.3	58.8	149.1 / 155.2	25.2	2.3
PLLA/SiO ₂ /PEG (90/10/5)	109.5	-24.6	56.3	147.6 / 155.5	27.6	3.8
PLLA/SiO ₂ /PEG (90/10/8)	101.8	-23.2	51.2	144.3 / 153.8	28.2	6.4
PLLA/SiO ₂ /PEG (90/10/10)	99.8	-23.3	49.6	143.8 / 153.7	28.2	6.5

6.3 Equilibrium melting temperature determination

As described in the characterization section, the samples were isothermally crystallized and immediately heated to record their melting behavior. Figure 4 (a) shows a representative example of DSC heating scans for the PLLA/SiO₂ (90/10) composite. For the different isothermal crystallization temperatures used, two melting peaks were identified. In the literature, Yasuniwa (65) ascribed the double-melting property of isothermally crystalline PLLA to melt-recrystallization. Figure 4 (b) depicts a typical Hoffman-Weeks (HW) plot for the Figure 4 (a). Melting peak I can be observed to be dependent on T_c , but melting peak II demonstrated significantly less dependency on the isothermal temperature. T_m values corresponding to the lower-temperature endothermic peak were collected after more than 10 min of isothermal crystallization to avoid data divergence caused by secondary crystallization, lamellar thickening, and crystallization perfection. Figure 4 (b) depicts the generated T_m and T_c data. T_m^0 is often calculated by linearly extrapolating the T_m vs. T_c plot to the line $T_m = T_c$, as stated by linear Hoffman-Weeks (HW) extrapolation.

A peculiarity was found in the behavior of peak I of PLLA/SiO₂/PEG (90/10/5), PLLA/SiO₂/PEG (90/10/8), and PLLA/SiO₂/PEG (90/10/10) composites. In these three cases, the enthalpy of fusion of the fusion peak I decrease with decreasing isothermal

crystallization temperature. This behavior is much more visible in the case of PLLA/SiO₂/PEG (90/10/10) since it has the lowest isothermal crystallization temperatures. The lowest crystallization temperatures for that composite were 82, 80, and 78 °C, the behavior of the peak I may be described using the melt/recrystallization mechanism. The melting of original crystals that form after cooling may combine with the higher (re-crystallization) exotherm, resulting in the disappearance of the low-temperature melting peak I at 82 °C or less (72). Nevertheless, the melting I peaks could be slightly distinguished. These were used to calculate the equilibrium melting point by the HW procedure.

The equilibrium melting temperature is taken from the literature (51,52), estimated to be 480 K and 479 K estimated by (73). The values of the equilibrium melting temperatures obtained for all of the samples are shown in Table 3. Trends in T_m^0 are observed; for the composites with silica, it decreases from 180 to 175 °C for the one containing 10 wt%, while it increases to 184 °C for the one containing 15 wt%. It is known that the glass transition temperature (T_g) and equilibrium melting temperature (T_m^0) are primary factors that influence the crystallization rate of a polymer (8). Because of the high silica concentration added, the equilibrium melting temperature increases. As a result, as aforementioned, nucleation is favored. Even though these T_m^0 values are lower than those reported in the literature, the thickening ratio (γ) are between 2 and 3 by linear HW extrapolation (74), and it is concluded that linear HW extrapolation is applicable in T_m^0 determination PLLA composites. Furthermore, T_m^0 values for composites containing silica and PEG grow dramatically from 169 to 215°C as the quantity of PEG in the composite increases, as predicted. This increase in T_m^0 is expected since, as mentioned above, incorporating PEG into the composites improves the crystallization rate by increasing crystallization's driving force (8). Concerning the values of γ , no variations are observed in those composites that contain silica. However, a decreasing trend is seen in the composites with PEG content. The value of γ decreases with the content of PEG, which implies that lower lamellar thickness is needed to enable the secondary surface nucleation and growth.

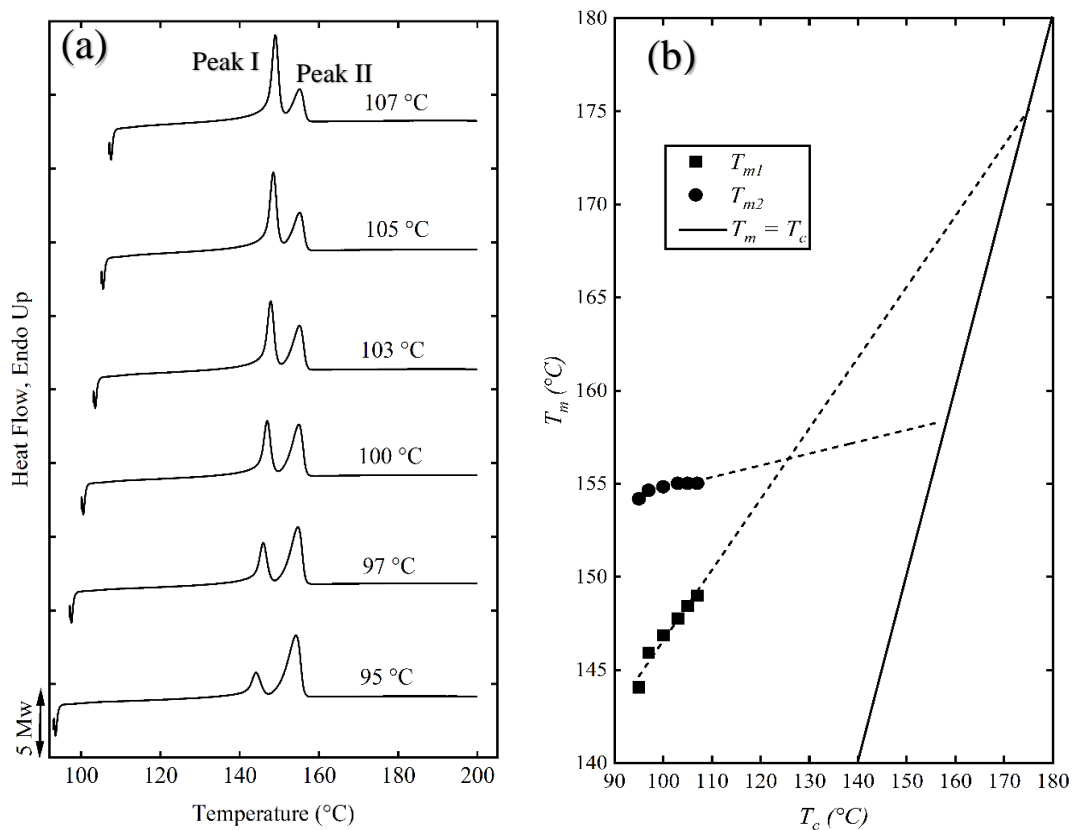


Figure 4. a DSC heating scans after isothermal crystallization at the indicated temperatures for the PLLA/SiO₂ (90/10) composite. b Hoffman–Weeks plot for the same composite.

Table 3. Variation of T_m^0 with the content of SiO₂ and PEG determined by Hoffman–Weeks extrapolation procedure.

Sample	T_m^0 (°C) (H-W)	γ
PLLA	180	2.4
PLLA/SiO ₂ (95/5)	180	2.3
PLLA/SiO ₂ (90/10)	175	2.6
PLLA/SiO ₂ (85/15)	184	2.4
PLLA/SiO ₂ /PEG (90/10/3)	169	3.2
PLLA/SiO ₂ /PEG (90/10/5)	198	1.9
PLLA/SiO ₂ /PEG (90/10/8)	199	1.9
PLLA/SiO ₂ /PEG (90/10/10)	215	1.7

6.4 Isothermal crystallization kinetics

Figure 5 shows experimental data for the overall crystallization rate of PLLA composites as a function of isothermal crystallization temperature T_c . Figure 5 shows that the overall crystallization rate is a function of the PEG concentration of the composites and the crystallization temperatures. For those reasons, it is essential to detect the difference between the PLLA/SiO₂ and the PLLA/SiO₂/PEG composites. The T_c required for crystallization increases somewhat as SiO₂ concentration increases, implying that supercooling decreases. In contrast, the T_c required for crystallization of PLLA/SiO₂/PEG composites is lower, implying an increase in supercooling. This relates to the results presented above that PEG has high miscibility in PLLA, increasing the mobility of PLLA chains and crystallization rate. Similarly, it was predicted that the crystallization of the PLLA/SiO₂ composites with a silica concentration of 15% would occur at a higher T_c . The lower crystallization rate of PLLA containing 15% silica may be described as follows: increasing the filler loading inhibits the PLLA chain motion, raising the energy barrier for spherulite development (75). The consequence is an overall decrement in the rate of crystallization. In addition, it is essential to note that the values of half-crystallization time increase as the crystallization temperature decreases. This behavior occurs due to the proximity of the crystallization temperatures used since it is known that crystallization is slower near T_g and T_m . Figure 6 depicts the values half-crystallization time concerning SiO₂ and PEG content. As a result of the low chain mobility (60), the inverse of half-crystallization time decreases as SiO₂ content increases. On the other hand, increasing the PEG increases the mobility of the chain, allowing us to observe high values of half-crystallization time at lower crystallization temperatures.

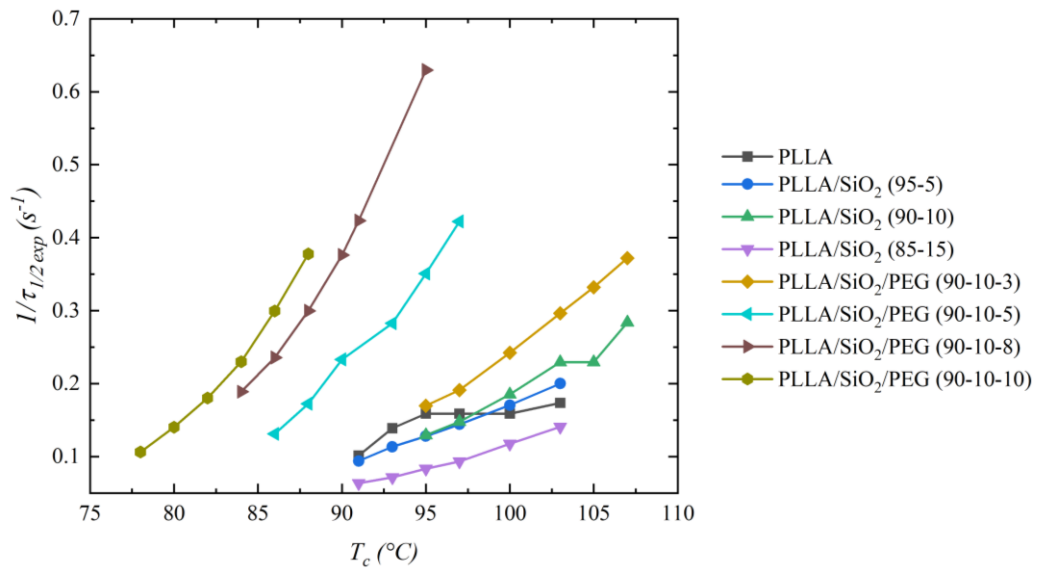


Figure 5. Dependence values of the inverse of $\tau_{1/2exp}$ as a function of the isothermal crystallization temperature for the composites.

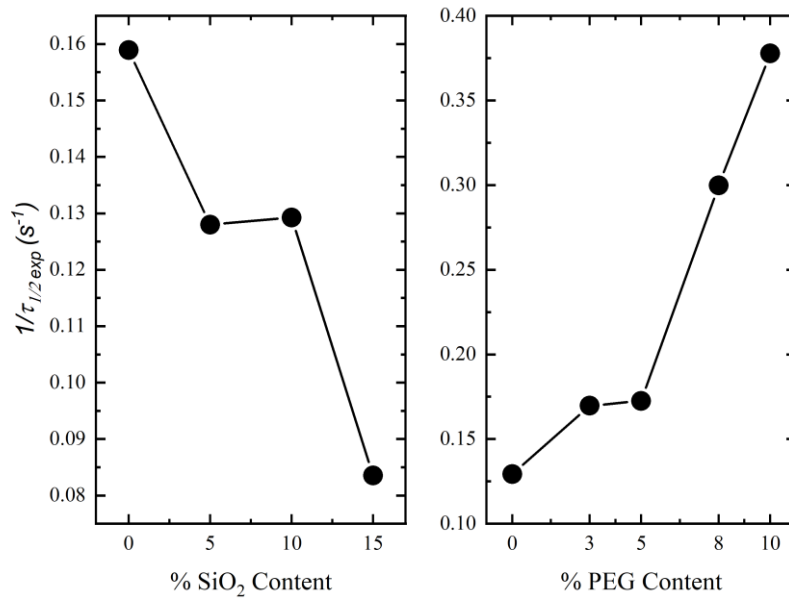


Figure 6. Values of the inverse of $\tau_{1/2exp}$ at 95°C for PLLA/SiO₂ and 88°C for PLLA/SiO₂/PEG composites

Table 4 presents the results obtained from the Avrami fit (Eq. 2) (47,48). Two examples are supplied to demonstrate the fitting range: PLLA and two composites, one with silica (PLLA/SiO₂ (95/5)) and one with silica and PEG (PLLA/SiO₂/PEG (90/10/3)). We used the Avrami theory to fit the isothermal DSC data in a 5-20% conversion range, which corresponds to the primary crystallization range where the Avrami analysis is most appropriate. It is important to note that the conversion range is typically 3-20%; we adjust this range to get more accuracy over 0.9990 for R² to indicate a very excellent fit of the data in a specific conversion range (47) Figure 7 and 8 demonstrates how the Avrami fit (solid line) perfectly reflects the experimental data up to 50% conversion. Figure 9 compares the Avrami-derived DSC curve to the experimental data, and the fit is excellent on the left side of the DSC curve or within the primary crystallization region.

As a typical semicrystalline polymer, PLLA crystallizes slowly at temperatures near the melting and glass transition temperature (49). The values of *k*, the overall crystallization rate constant, follow a trend similar to the one seen in Figure 5. The higher values of the isothermal crystallization parameter *k* given in Table 4 verified the increase in chain mobility caused by adding PEG to PLLA/SiO₂ composites. The predicted Avrami values of half-crystallization time are highly similar to the experimental values in most cases, as expected from the trends shown in Figure 7.

Table 4. Avrami fitting parameters (*n*, *K*, $\tau_{1/2}theo$) and their correlation coefficient *R*². The experimental value of $\tau_{1/2}$ is given for comparison purposes. The conversion range employed was the same in every case, 5–20%.

Sample	T (°C)	n	K (min ⁻ⁿ)	$\tau_{1/2}theo$ (min)	$\tau_{1/2}exp$ (min)	R ²
PLLA	91	3.27	3.42E- 04	10.25	9.87	0.9992
	93	3.32	9.76E- 04	7.23	7.20	0.9999
	95	3.68	8.32E- 04	6.22	6.29	1.0000
	97	4.00	5.13E- 04	6.06	6.18	1.0000
	100	3.68	7.75E- 04	6.14	6.33	1.0000
	103	3.56	1.56E- 03	5.56	5.76	0.9999

Table 4. Continuacion

Sample	T (°C)	n	K (min ⁻ⁿ)	$\tau_{1/2}^{theo}$ (min)	$\tau_{1/2}^{exp}$ (min)	R ²
PLLA/SiO ₂ (95/5)	90	3.61	1.34E- 04	10.66	10.52	0.9999
	91	3.64	1.19E- 04	10.80	10.64	0.9996
	93	3.77	1.87E- 04	8.83	8.82	0.9998
	95	3.87	2.51E- 04	7.73	7.81	0.9999
	97	3.78	5.05E- 04	6.76	6.93	1.0000
	100	3.61	1.29E- 03	5.70	5.87	1.0000
PLLA/SiO ₂ (90/10)	95	3.75	3.21E- 04	7.76	7.74	0.9998
	97	3.59	7.08E- 04	6.81	6.76	0.9997
	100	3.45	2.05E- 03	5.41	5.39	0.9998
	103	3.32	5.28E- 03	4.40	4.36	0.9998
	105	3.32	4.86E- 03	4.46	4.42	0.9998
	107	3.28	1.07E- 02	3.57	3.53	0.9998
PLLA/SiO ₂ (85/15)	91	4.16	8.18E- 06	15.29	15.73	1.0000
	93	4.21	1.28E- 05	13.36	13.95	0.9999
	95	3.74	7.17E- 05	11.64	11.97	1.0000
	97	3.48	1.97E- 04	10.41	10.70	1.0000
	100	3.24	7.10E- 04	8.37	8.51	1.0000
	103	3.02	1.91E- 03	7.06	7.11	1.0000
PLLA/SiO ₂ /PEG (90/10/3)	95	3.60	1.26E- 03	5.77	5.89	1.0000
	97	3.49	2.57E- 03	4.97	5.24	1.0000
	100	3.37	7.34E- 03	3.86	4.13	1.0000
	103	3.26	1.67E- 02	3.13	3.37	1.0000
	105	3.23	2.47E- 02	2.81	3.01	1.0000
	107	3.17	3.68E- 02	2.52	2.69	1.0000
PLLA/SiO ₂ /PEG (90/10/5)	86	3.08	1.18E- 03	7.90	7.63	0.9996
	88	3.13	2.52E- 03	6.02	5.80	0.9994
	90	3.15	6.15E- 03	4.48	4.29	0.9993
	93	3.08	1.27E- 02	3.66	3.54	0.9993
	95	3.06	2.54E- 02	2.95	2.85	0.9994
	97	3.04	4.58E- 02	2.44	2.37	0.9995

Table 4. Continuacion

Sample	T (°C)	n	K (min ⁻ⁿ)	$\tau_{1/2}^{theo}$ (min)	$\tau_{1/2}^{exp}$ (min)	R ²
PLLA/SiO ₂ /PEG (90/10/8)	84	3.06	3.30E- 03	5.74	5.29	0.9990
	86	3.15	5.87E- 03	4.56	4.24	0.9990
	88	3.21	1.19E- 02	3.54	3.34	0.9992
	90	3.19	2.55E- 02	2.82	2.66	0.9992
	91	3.24	3.59E- 02	2.49	2.36	0.9994
	95	2.98	1.43E- 01	1.70	1.59	0.9991
PLLA/SiO ₂ /PEG (90/10/10)	78	3.04	6.80E- 04	9.78	9.41	0.9993
	80	3.05	1.52E- 03	7.44	7.13	0.9991
	82	3.16	2.78E- 03	5.72	5.55	0.9995
	84	3.20	5.78E- 03	4.47	4.35	0.9996
	86	3.24	1.30E- 02	3.41	3.34	0.9998
	88	3.30	2.64E- 02	2.69	2.65	0.9998

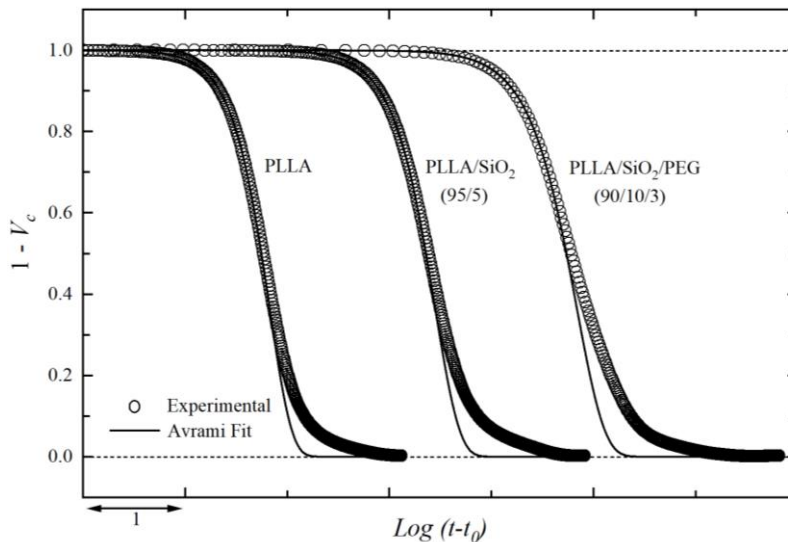


Figure 7. Variation of $1 - V_c$ (volumetric relative amorphous content) with $\log(t - t_0)$. A comparison between the experimental data and the fitting of the Avrami Eq. 2 for the indicated samples. The crystallization temperatures were 97, 100 and 107 °C for the PLLA, PLLA/SiO₂ (95/5) and PLLA/SiO₂/PEG (90/10/3) respectively.

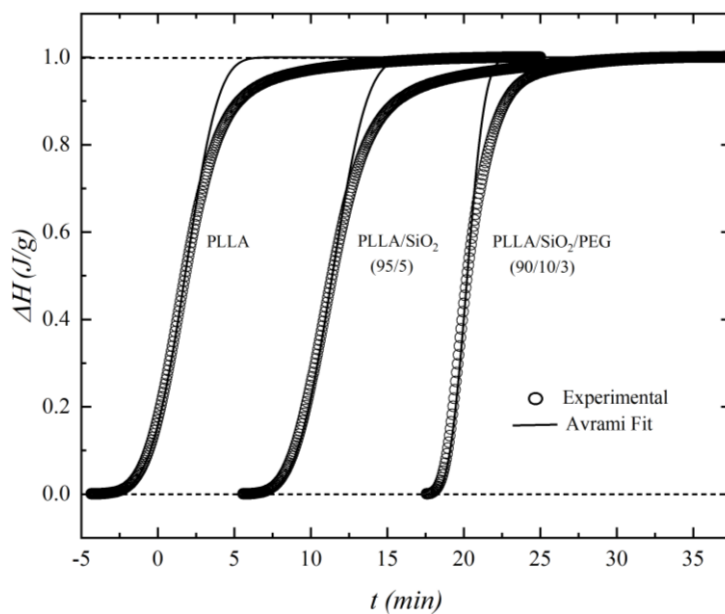


Figure 8. Variation of the enthalpy of crystallization (ΔH_c) with time (t) for PLLA, PLLA/SiO₂ (95/5) and PLLA/SiO₂/PEG (90/10/3) composites.

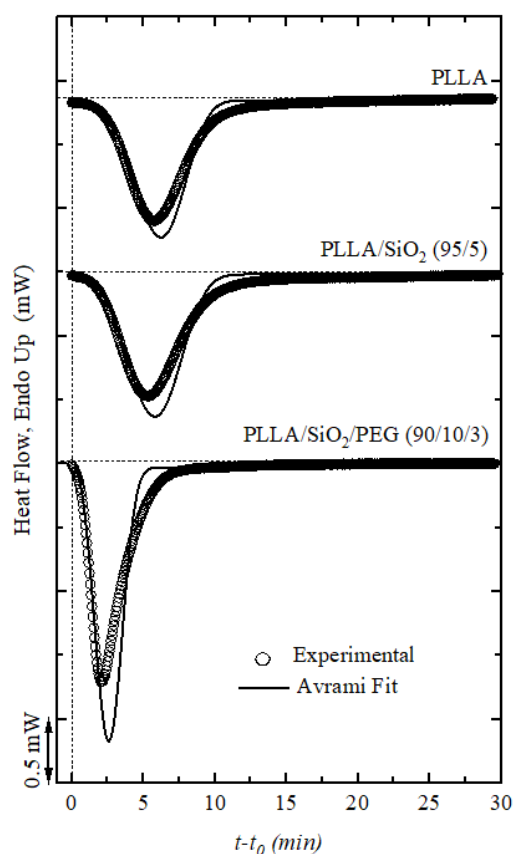


Figure 9. Experimental DSC isotherms and simulated DSC curves by the Avrami equation for the PLLA, PLLA/SiO₂ (95/5) and PLLA/SiO₂/PEG (90/10/3) composites. The crystallization temperatures were 97, 100 and 107 °C for the PLLA, PLLA/SiO₂ (95/5) and PLLA/SiO₂/PEG (90/10/3), respectively.

Figure 10 presents the values of n versus the isothermal crystallization temperatures. The value of n is associated with the nucleation type present during the experiment, according to Lorenzo et al. (47). Changes in n indicate that conditions such as the presence of the plasticizer PEG, its concentration, and the crystallization temperature have a strong influence on the crystallization mechanism of PLLA. n values in the range of 3-4 obtained for PLLA/SiO₂ composites indicate mainly heterogeneous nucleation with three-dimensional sporadic crystal growth. These n values were favored in the presence of filler (63) at higher crystallization temperatures since 91°C. In contrast, n values close to 3 obtained for PLLA/SiO₂/PEG composites indicate that a particular concentration of PEG favored three-dimensional instantaneous crystal growth at lower temperatures from 78°C. PEG interacts with polymer chains, increasing its mobility and accelerating viscoelastic response (76).

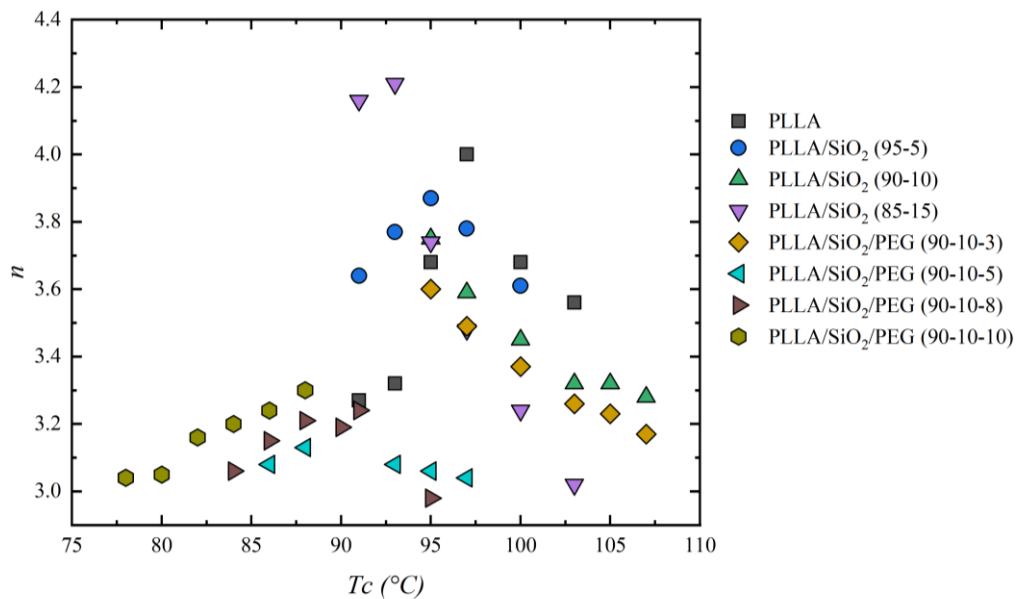


Figure 10. Avrami index (n) versus isothermal crystallization temperature (T_c) for the indicated samples.

Table 5 shows the parameters calculated with Lauritzen and Hoffman (L-H) theory Eq. 3 (50–52,54–56). For the composite containing 15 wt% silica, the value of σ_e rises, demonstrating that excessive silica addition has no beneficial impact on crystallization kinetics and may even to impede crystallization to some extent, due to the

impeding effect of significant silica loadings (54). In contrast, it is observed how the values of σ_e decrease drastically with the increase of PEG, indicating that the plasticizer improves the nucleation and mobility of the PLLA chains (75), and decreases the lamellar thickness (49).

In the values obtained for q , and σ_e a definite declining trend can be seen. In this work we employ the values of $1/\tau_{1/2}$ and $Z = 4$ as a measure of crystallization rate for the crystallization regime. The results are shown in Table 5. The results suggest that the PEG presence lowered the work required for PLLA chains to fold into the crystal. This phenomenon may occur due to the crystals' decreasing size or degree of perfection (49). PEG improved polymer chain mobility and accelerated crystallization by lowering the energy required for the chain folding process during crystallization (76,77). However, there was a slight increase in chain folding for the composite PLLA/SiO₂/PEG (90/10/10); this behavior might be linked to some PEG being trapped in the intraspherulitic region of PLLA, inhibiting PLLA crystallization (78).

Table 5. Kinetics results of PLLA composites obtained by using Lauritzen–Hoffmann equation 3.

Sample	K_g	$\sigma_e * 10^{-3}$ (J^2/m^4)	q (KJ/mol)	Regime
PLLA	9.67E+05	96.9	36.02	<i>III</i>
PLLA/SiO ₂ (95/5)	8.36E+05	83.8	31.16	<i>III</i>
PLLA/SiO ₂ (90/10)	5.75E+05	57.7	21.44	<i>III</i>
PLLA/SiO ₂ (85/15)	8.03E+05	80.5	29.92	<i>III</i>
PLLA/SiO ₂ /PEG (90/10/3)	5.18E+05	51.9	19.29	<i>III</i>
PLLA/SiO ₂ /PEG (90/10/5)	6.17E+05	61.9	23.01	<i>III</i>
PLLA/SiO ₂ /PEG (90/10/8)	4.54E+05	45.5	16.90	<i>III</i>
PLLA/SiO ₂ /PEG (90/10/10)	5.18E+05	51.9	19.29	<i>III</i>

According to L-H's secondary nucleation theory, polymers crystallize in three distinct regimes (50). The lateral spreading rate is much greater than the surface nucleation rate at the lowest undercooling when regime I is found. The rates of the two processes are equivalent to moderate undercooling when regime II is seen. Secondary

nucleation is faster than lateral spreading at the greatest undercooling when regime III is present (49,72). A regime II-III transition has been reported for PLLA at about 115 °C (73) and 120 °C (53). This work used crystallization temperatures between 78-107 °C that are crystallization covered regime III; as shown in Figures 11 and 12, the samples do not present the change from regime III to regime II. In regime III thin lamellar crystals are present at high undercooling and characterized by irregular surface. With decreasing temperature, the nucleation rate increases continuously. As a result, at low temperatures, which means big undercooling, the rate is fast, and the nuclei are many and small in size (79). As a result, there is not much space for the nuclei to expand and develop.

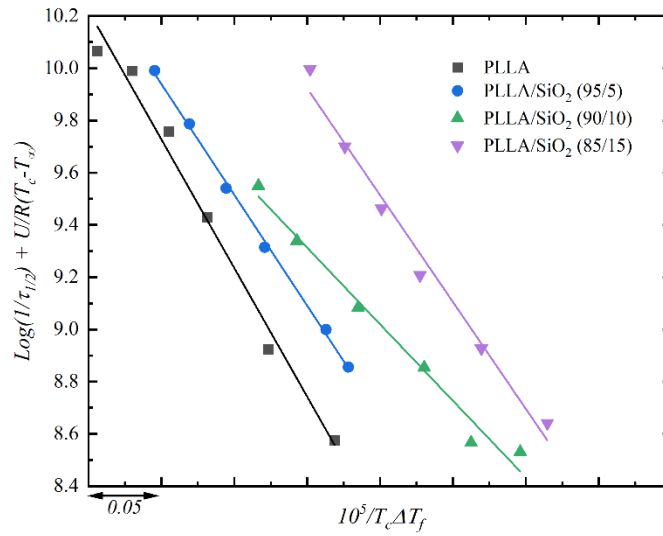


Figure 11. Plots of $\ln(1/t_{1/2}) + U^*/R(T_c - T_\infty)$ versus $(1/T_c\Delta T_f)$ for PLLA, PLLA/SiO₂ (95/5), PLLA/SiO₂ (90/10) and PLLA/SiO₂ (85/15) composites.

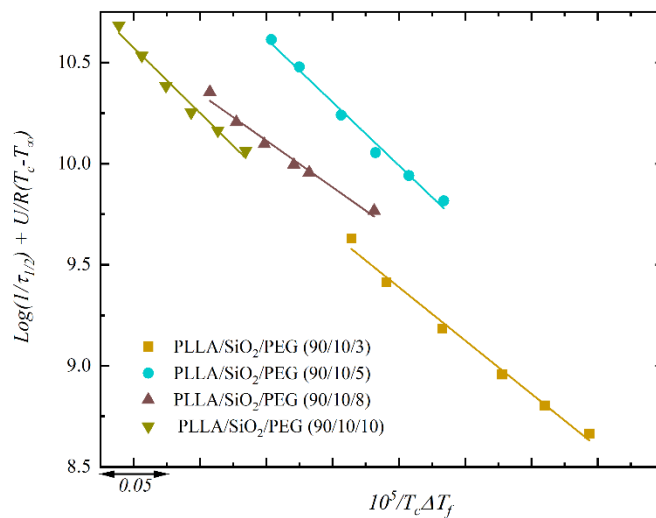


Figure 12. Plots of $\ln(1/t_{1/2}) + U^*/R(T_c - T_\infty)$ versus $(1/T_c\Delta T_f)$ for PLLA/SiO₂/PEG composites.

6.5 Thermal Stability

The thermogravimetric analysis (TGA) of PLLA, PLLA/SiO₂, and PLLA/SiO₂/PEG composites were used to study their thermal stability and its relationship with crystallinity, which are shown in Figure 13 (a). Figure 13(b) depicts the weight loss and its derivative (DTA) against temperature curves for PLLA composites, which give information regarding the tested materials' mechanism and level of degradation. The onset temperature (onset T) and maximum thermal degradation rate (degradation T) were calculated using Figure 13 (a) and presented in Table 6. Figure 13 (a) shows that the incorporation of SiO₂ content increased the initial thermal stability of the composites due to the addition of silica made removing volatile components from the structure difficult, and the thermal decomposition temperature began to rise (28).

On the other hand, PEG allows the chain segments to move easily and improves the flexibility of PLLA (28,80). PEG concentration lowers the PLLA degradation temperature because PEG has a lower thermal degradation temperature than PLLA. This behavior is more visible for composites with 8 and 10 wt% of PEG. Also, as PEG concentration increased, PLLA lubrication became the primary mechanism facilitating heat degradation (15).

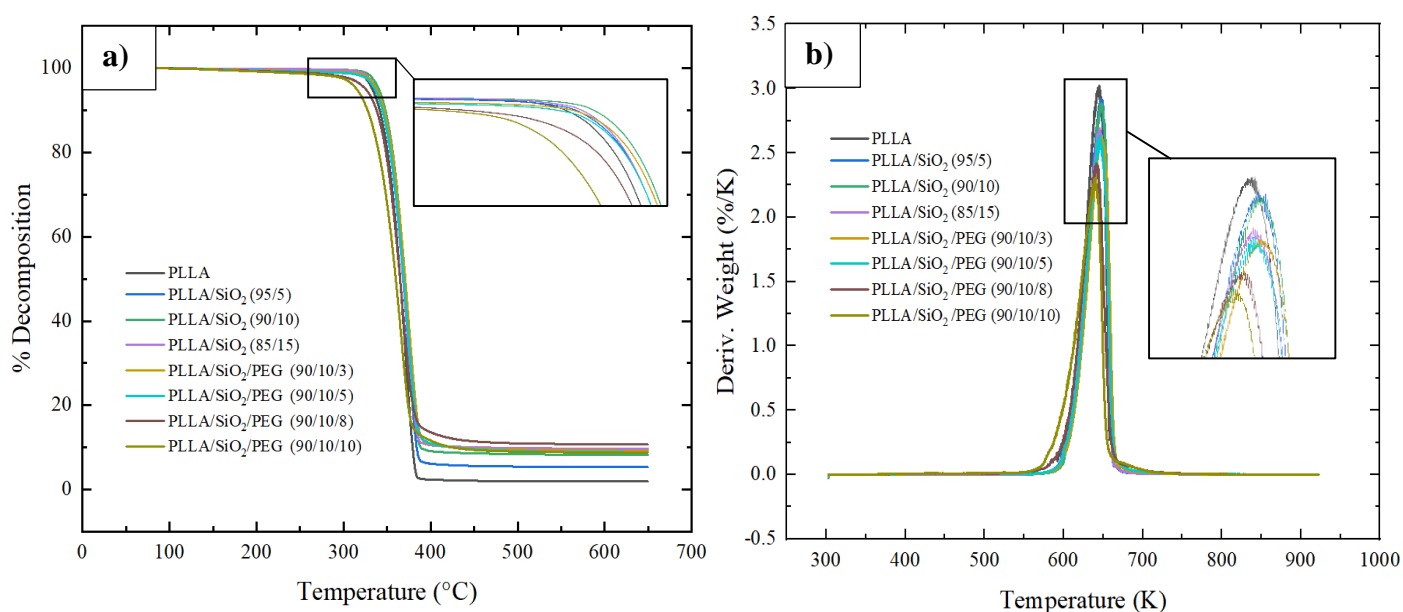


Figure 13. (a) Thermogravimetric analysis (TGA) and its (b) Differential Thermogravimetric Analysis (DTA) curves of PLLA, PLLA/SiO₂ and PLLA/SiO₂/PEG composites.

Table 6. TGA results of PLLA, PLLA/SiO₂ and PLLA/SiO₂/PEG composites at heating rate of 10 °C/min.

Sample Code	Onset T (°C)	Endset T (°C)	Degradation T (°C)	Total W. Loss (%)
PLLA	344.66	380.74	364.15	98.82
PLLA/SiO ₂ (95/5)	346.03	384.85	368.94	94.72
PLLA/SiO ₂ (90/10)	350.99	385.02	369.97	91.79
PLLA/SiO ₂ (85/15)	346.20	383.21	368.77	91.22
PLLA/SiO ₂ /PEG (90/10/3)	347.74	386.90	369.97	90.82
PLLA/SiO ₂ /PEG (90/10/5)	350.14	385.02	368.77	91.19
PLLA/SiO ₂ /PEG (90/10/8)	341.07	381.25	365.01	90.35
PLLA/SiO ₂ /PEG (90/10/10)	332.35	378.18	359.88	89.33

Using the Friedman method (Eq. 6), the calculated results of kinetic parameters for thermal degradation of all composites at 10 °C/min are given in Table 7. The values presented are obtained by plotting $\ln(da/dt)$ versus $(1/T)$ with the slope (E_a/R) for calculating the values of E_a . The order of the reaction (n) for PLLA is 1.3. The E_a value for pure PLLA is 201.631 kJ/mol, higher than the literature, approximately 161 kJ/mol (66,81). The E_a value difference can be explained as follows. Friedman's method is well known for being very sensitive to experimental noise and numerically unstable due to the use of instantaneous rate value (82). However, it is clear that there is a trend in the E_a of PLLA composites, suggesting that the SiO₂ added to the polymer matrix have led to greatly increased E_a and resulted in a substantially higher thermal stability. Otherwise, PEG composites have low E_a values, indicating lower thermal stability and corroborating the data obtained by TGA.

Table 7. Kinetic parameters of PLLA, PLLA/SiO₂ and PLLA/SiO₂/PEG composites at heating rate of 10 °C/min according Eq. 6.

Sample	E _a (KJ/mol)	n	Ln(A)	R ²
PLLA	201.631	1.3	39.183	0.992
PLLA/SiO ₂ (95/5)	212.248	1.7	41.027	0.993
PLLA/SiO ₂ (90/10)	247.923	1.1	47.838	0.995
PLLA/SiO ₂ (85/15)	218.791	1.3	42.356	0.990
PLLA/SiO ₂ /PEG (90/10/3)	241.455	1.2	46.566	0.992
PLLA/SiO ₂ /PEG (90/10/5)	227.895	1.2	44.073	0.994
PLLA/SiO ₂ /PEG (90/10/8)	214.734	1.0	41.769	0.993
PLLA/SiO ₂ /PEG (90/10/10)	156.428	0.9	30.687	0.994

6.6 Melt Rheology

Determining system rheological properties is important because adding solid particles to a molten polymer can change its viscoelastic behavior and elasticity (83). At the processing temperature of 190 °C, the rheological behavior of PLLA and PLLA composites was measured, and the results are shown in Figure 14. In general, the frequency significantly impacts how the complex viscosity (η^*) changes. Because of the shear thinning characteristic, it was possible to see in Figure 14(a) that the η^* of all the samples decreased with angular frequency (ω) (84). PLLA exhibited normal non-newtonian behavior (85), and η^* of PLLA/SiO₂ composites rise when 5, 10, and 15 wt% silica was added (Figure 14(a)). The addition of silica to the polymer matrix increased the viscosity of the system, most likely due to flow line disruption and restriction of polymer chain mobility (83). The presence of fillers increased the viscosity of the composites because a higher shear force is required to overcome stronger PLLA–filler interaction (86). Moreover, when additional silica is added the network configuration becomes stiffer, raising the storage modulus (G') (Figure 14(b)). Because the rheological properties at the low frequency (ω) regime reflect the relaxation and motion of the entire polymer chain, the storage modulus (G') at the low frequency (ω) regime is strongly dependent on the addition of fillers (87). The G' increases as silica loading increases, indicating stronger adhesion with the PLLA matrix. This is explained by the interaction of silanol groups in silica and hydroxyl end groups in PLA during melt processing (88). Figure 14(d) shows

the relationship of the $\tan\delta$ of all the composites as functions of the angular frequency, showing that PLLA/SiO₂ the values of $\tan\delta$ are larger than pure PLLA at lower frequencies because of the restricted chain mobility.

The complex viscosity steadily dropped as the PEG level increased, demonstrating that PEG has a remarkable impact of plastification of the PLLA/SiO₂ (90/10) composite. Figure 14(a) shows that increasing the PEG concentration in all PLA/SiO₂/PEG composites exhibits a more prominent non-newtonian response than pure PLLA. Increasing the PEG concentrations reduces the viscosity of the composites significantly (89). Because of the plasticizing impact of PEG, this would confirm the disentanglement and improve the segmental mobility of the PLLA chain (78). The complex viscosity of PLLA/SiO₂/PEG (90/10/10) was lowered by more than an order of magnitude compared to PLLA/SiO₂ (90/10), with a notable drop for plain PLLA. Figure 14(c) demonstrates that the Loss Modulus (G'') for all PEG samples was more significant than the Storage Modulus, suggesting that the materials were more viscous than elastic (90). The Storage and Loss Modulus of composites decreased with increasing PEG concentration compared to neat PLLA and PLLA/SiO₂ (90/10). These behaviors suggest that an enhancement filler reorientation in the flow direction and PLLA chain disentanglement. The diluting effect brought on by the plasticizer's presence could cause the PLLA/SiO₂/PEG composites' decreased viscosity and enhanced fluidity (91). Compared to pure PLLA and PLLA/SiO₂ composites at lower frequencies, the $\tan \delta$ value for PLLA/SiO₂/PEG composites was significantly lower. The value of $\tan \delta$ was reduced, indicating a faster melt response and greater melt flexibility. This behavior could be due to the chains' improved molecular mobility due to the addition of PEG to the PLLA matrix.

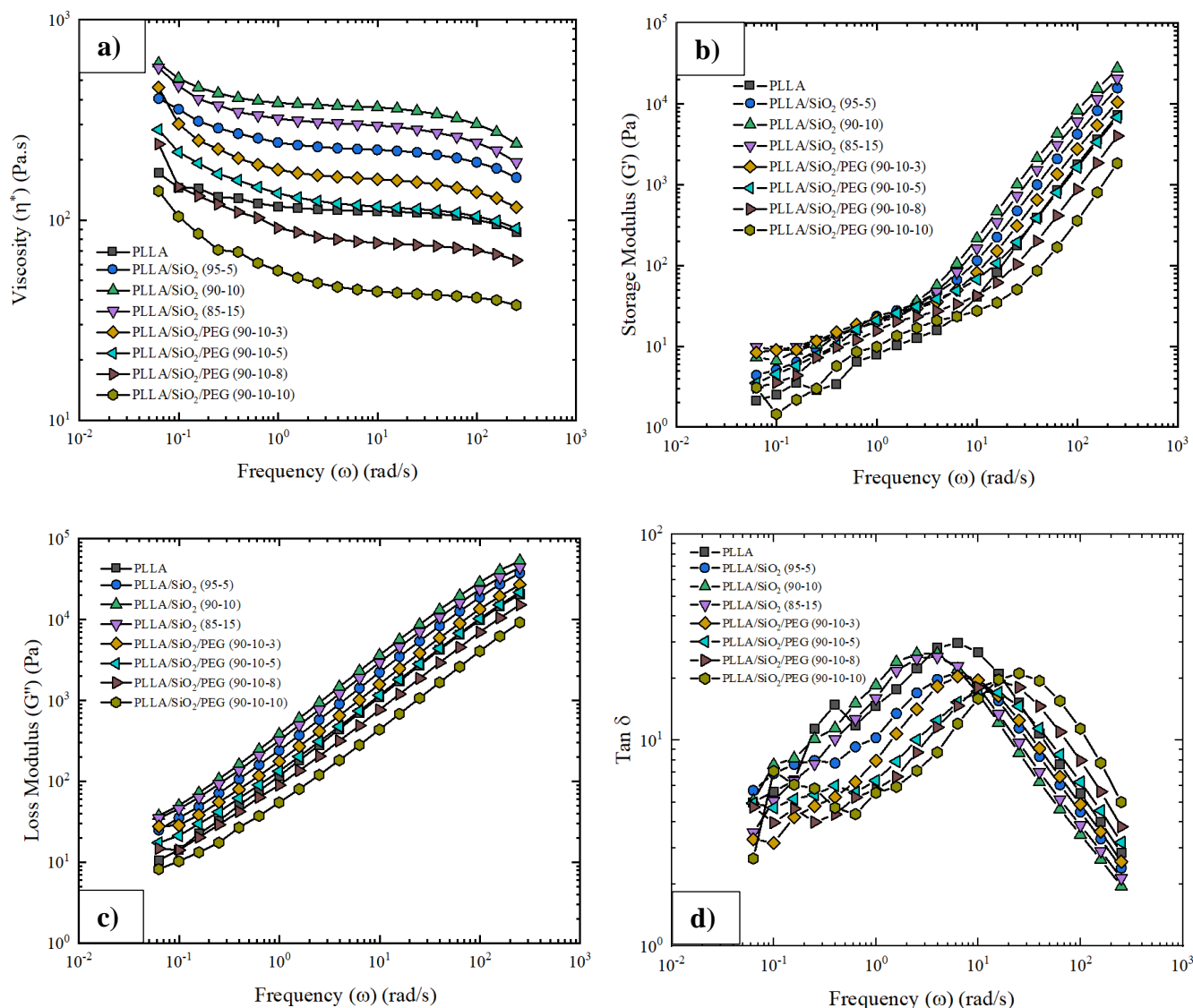


Figure 14. (a) Complex viscosity versus frequency, (b) Storage Modulus versus frequency (c) Loss Modulus versus frequency, (d) Damping factor (Tan δ) versus frequency for PLLA, PLLA/SiO₂ and PLLA/SiO₂/PEG composites at 190 °C.

6.7 Tensile Test

The tensile properties of pure PLLA and PLLA composites were examined, and the corresponding results are in Figure 15 and Table 8. PLLA has a high elastic modulus and tensile strength but is highly brittle, with only around 3-5 percent elongation at break (92). In order to improve their mechanical properties, SiO₂ was added as a filler. The interface between the filler particle and the polymer matrix significantly affects composites' tensile properties (93,94). The incorporation of SiO₂ in the PLLA matrix significantly decreases the tensile strength and elongation at the composites' break for all

the silica contents. Because there is no chemical bonding between the PLLA and SiO₂ particles, the composites' integrity is solely dependent on physical interactions between the filler and the polymer matrix.

Furthermore, thus load transfer at the PLLA/SiO₂ interface during tensile testing is inefficient, which is thought to be one of the reasons for the reduced tensile strength (95). Another explanation for the decrease in tensile strength is that, while the dispersion of SiO₂ in the PLLA matrix is relatively uniform for composites with 5 and 10 wt%, small agglomerates may negatively affect the tensile strength. For PLLA/SiO₂ composite with 15 wt%, the saturation and poor dispersion of SiO₂ negatively affect both Young's modulus and tensile strength. However, Young's modulus increased 12% for 5 wt% of silica and 26% for 10 wt%. This behavior is expected for fillers due to the reinforcing effect of particles (96,97) and the higher crystallinity that these composites present in comparison with the neat PLLA. The improved compression modulus of PLLA composites, on the other hand, can be explained by an interconnected SiO₂ particle network in the PLLA matrix (98), which can transmit load more efficiently through direct particle contact in the matrix.

In order to compensate for the brittleness introduced by incorporating SiO₂, PEG was added as a plasticizer. As an effective PLLA plasticizer, PEG promotes PLLA segment mobility and plastic elongation (92). Figure 10(b) shows that adding PEG to the composite PLLA/SiO₂ (90/10) decreases Young's Modulus and increases elongation at the break as the PEG content increases. These results confirm the plasticizer effect of PEG increasing the homogeneous dispersion of SiO₂ in the matrix, producing less stiffness in the composite, decreasing Young's modulus (17), and increasing the elongation at break of composites in comparison with PLLA/SiO₂ composites. Furthermore, Table 8 shows that the crystallinity of the samples increases as the PEG content increases. This enhancement is because plasticizers might enhance elongation at the break while decreasing tensile strength and tensile modulus, which led to a significant drop in the T_g . Plasticizers produce soft and flexible polymers by changing T_g and allowing intramolecular interactions between polymer and plasticizer, such as hydrogen bonding (13). There is an improvement in the elongation at break compared to the PLLA/SiO₂ (90/10) composite. However, to obtain more significant improvements in tensile strength and elongation at break, the amount and molecular weight of PEG must be increased, as reported by (13,16,17,89).

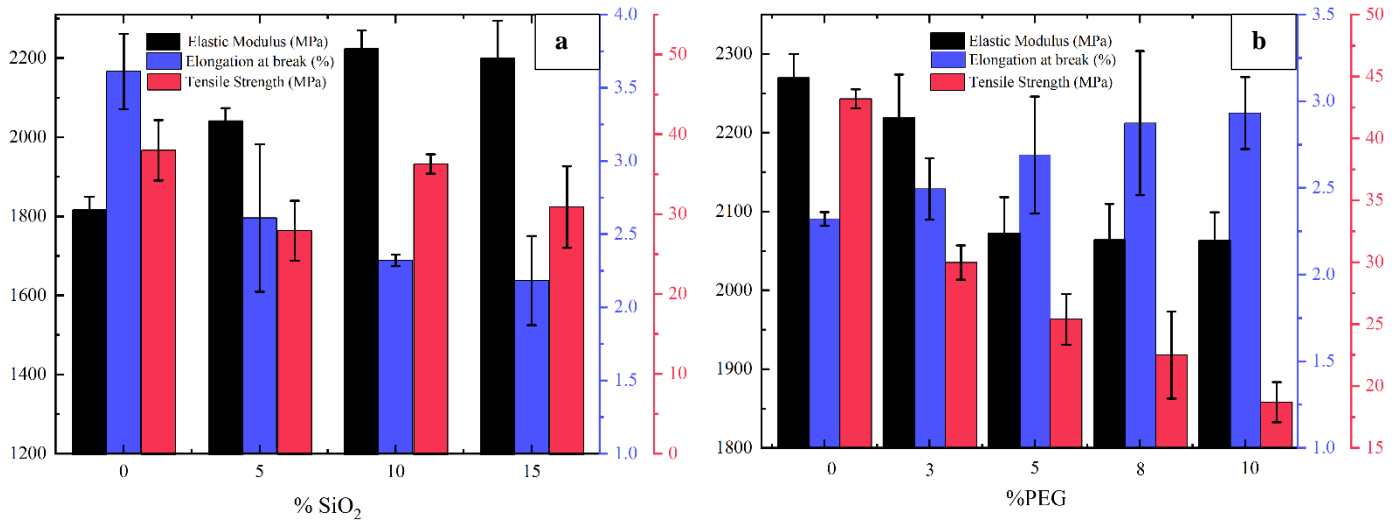


Figure 15. The mechanical properties: elastic modulus, tensile strength and elongation at break of (a) PLLA, PLLA/SiO₂ and (b) PLLA/SiO₂/PEG composites.

Table 8. Mechanical Properties of PLLA, PLLA/SiO₂ and PLLA/SiO₂/PEG composites.

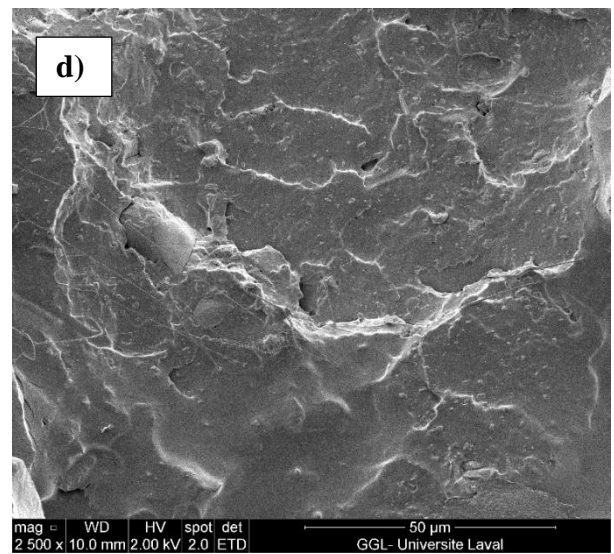
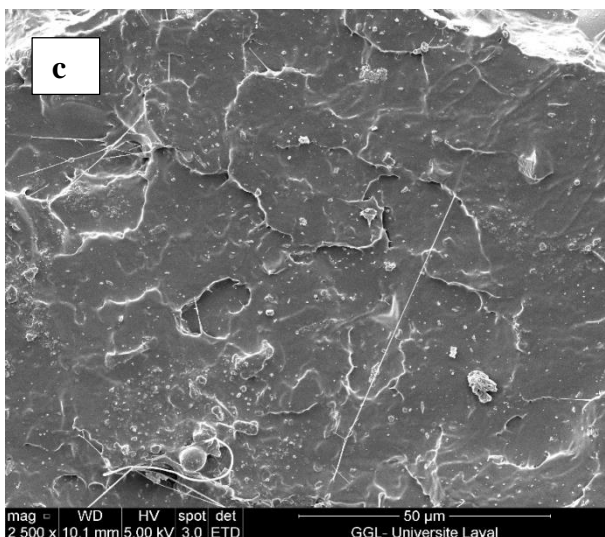
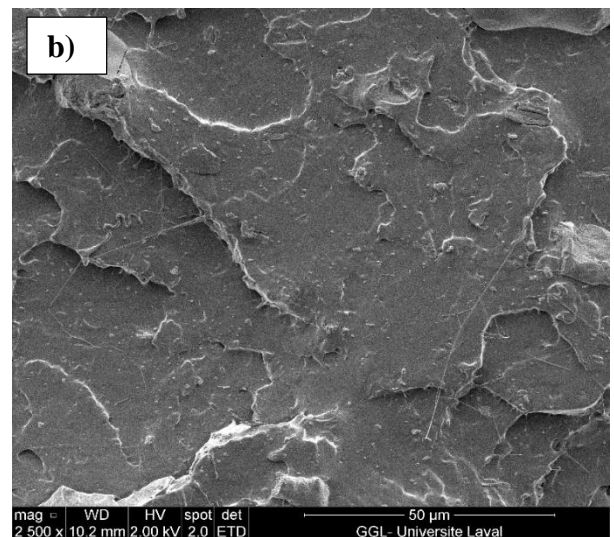
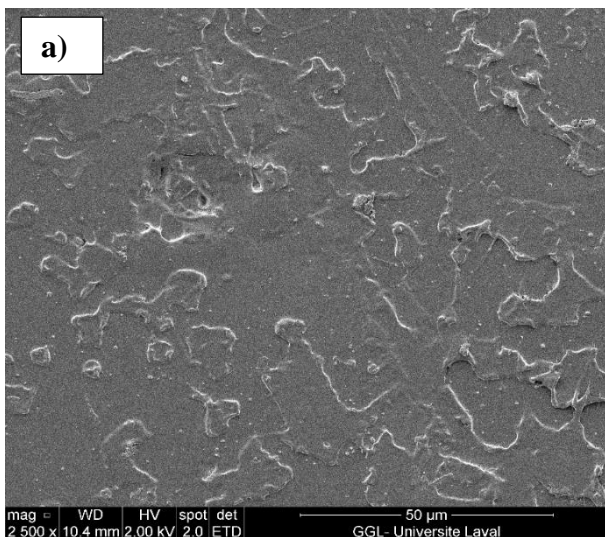
Sample	Elastic Modulus		Elongation at break		Tensile Strength	
	(MPa)		%		(MPa)	
PLLA	1818.69	± 33.59	3.61	± 0.26	44.28	± 2.41
PLLA/SiO ₂ (95/5)	2044.16	± 32.23	2.61	± 0.39	37.87	± 2.39
PLLA/SiO ₂ (90/10)	2292.00	± 46.46	2.32	± 0.04	43.18	± 0.78
PLLA/SiO ₂ (85/15)	2202.83	± 94.64	2.18	± 0.30	39.76	± 3.25
PLLA/SiO ₂ /PEG (90/10/3)	2148.37	± 84.25	2.49	± 0.18	29.96	± 1.38
PLLA/SiO ₂ /PEG (90/10/5)	1921.98	± 70.26	2.69	± 0.34	25.38	± 2.04
PLLA/SiO ₂ /PEG (90/10/8)	1908.56	± 81.10	2.87	± 0.70	22.49	± 3.51
PLLA/SiO ₂ /PEG (90/10/10)	1907.40	± 55.13	2.93	± 0.21	18.69	± 1.61

6.8 Surface rupture morphology

As it is well-known, fracture surfaces can reflect the mechanical properties of polymer composites. To further study the mechanical properties, the fracture surfaces of the tensile specimens were investigated by SEM and shown in Figure 16. Fracture surfaces of neat PLLA revealed features typical of brittle fracture of a glassy polymer with slight plastic deformation. Despicted in Figure 16(a) is shown a thin layer of the fractured surface, indicating brittle failure for neat PLLA (69). The micrographs from Figure 16(b) and

16(c) show a poor distribution of the SiO₂ and a similar brittle failure suggesting that matrix and filler do not interact enough; this trend also explains the mechanical properties of composites deteriorate as SiO₂ concentration rises. However, in Figure 16(d), it is seen that some fibrils and better distribution of SiO₂ may explain the increase in Young's modulus for PLLA/SiO₂ (90/10) composite. Adding a plasticizer (PEG) to micrographs 16(e) – 16(h) improves the filler and matrix interaction. PEG will promote the dispersion of SiO₂ in the PLLA matrix because it acts as a lubricant for the PLLA chains.

Furthermore, when the PEG concentration increases, the number of fibrils and their contact with SiO₂ increases, improving the matrix-load interaction. The thermal characteristics, like crystallization rate, directly impact the degree of crystallization and melting temperature. As a result, including PEG can improve filler/matrix adhesion enhancing thermal and mechanical properties as we explained above.



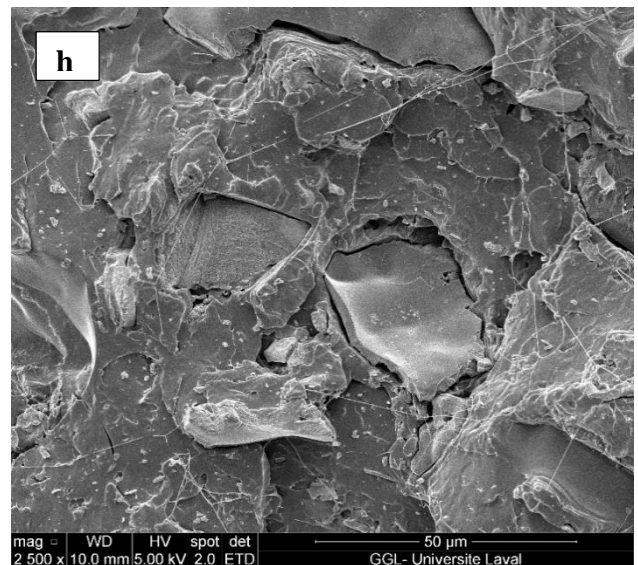
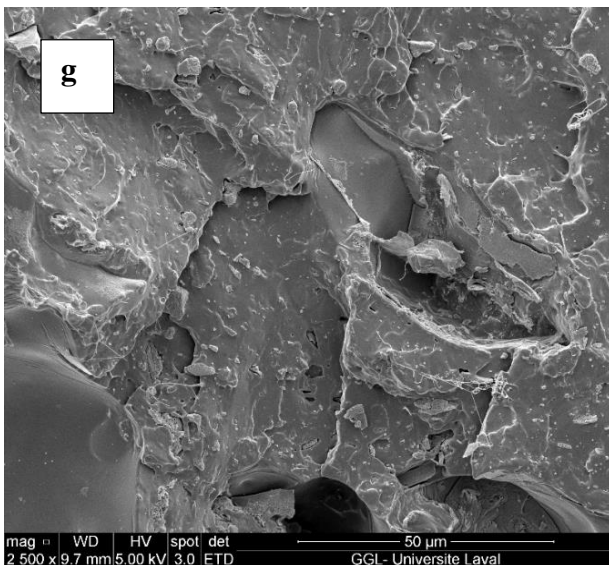
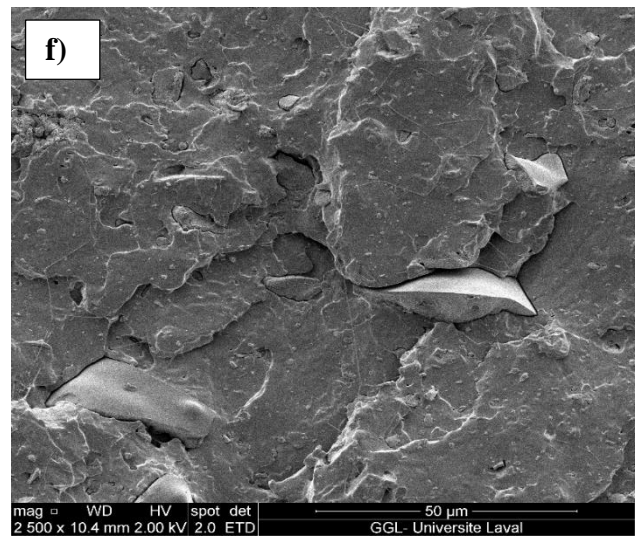
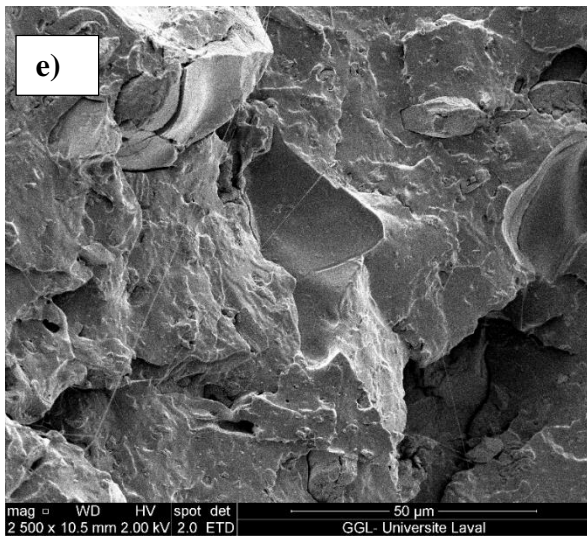


Figure 16. SEM micrographs of tensile test rupture surface of pure PLLA (a), PLLA/SiO₂ (95/5) (b), PLLA/SiO₂ (90/10) (c), PLLA/SiO₂ (85/15) (d), PLLA/SiO₂/PEG (90/10/3) (e), PLLA/SiO₂/PEG (90/10/5) (f), PLLA/SiO₂/PEG (90/10/8) (g), PLLA/SiO₂/PEG (90/10/10) (h).

6.9 X-Ray Diffraction Analysis

X-ray diffraction patterns were carried out to determine the crystal structures in the PLLA composites. The samples were thermally treated to enhance their crystallinity % and provide more accurate XRD patterns for the relevant analyses. In Figure 17 is shown the

XRD patterns of all composites, which contain four distinctive diffraction peaks corresponding to the (010), (200)/(110), (203), and (015) planes of PLLA according with the literature patterns (99,100). For PLLA/SiO₂ composites, there is no significant change in the shapes and position of the peaks. In contrast, when PEG was incorporated into the PLLA matrix since 3 wt%, the diffraction peaks became shaped-formed and shifted to higher positions. The peak in 16.3° representing the α' -crystalline phase with lower packing density due to incomplete crystallization (101). The intensity of this peak in systems with 10 wt% PEG increased and shifted to 16.6°. In addition, three more peaks appeared and shifted to higher positions: at $2\theta=14.7^\circ$, 18.7° , and 22.1° , corresponding to the lattice planes (200)/(100), (203) and (015), respectively, which are characteristic of the α -crystalline phase of PLLA (102)(103). The intensity of these peaks shows that plasticized PLLA composites have a greater capacity to generate α -crystalline structures. Table 9 shows the percentage of crystallinity determined using the XRD patterns. These values exhibits the same trend as the values calculated using the DSC data. They do not, however, demonstrate a significant rise in the DSC-obtained percentage crystallinity values as a consequence of the previous thermal treatment. As a result, we can suggest that the PEG content efficiently promotes the mobilization of the PLLA chains, which in turn enables the ordering of the PLLA chains and raises their crystallinity.

Table 9. Crystallinity Percent of PLLA, PLLA/SiO₂ and PLLA/SiO₂/PEG composites from XRD patterns.

Sample	Xc (%)
PLLA	33.51
PLLA/SiO ₂ (95/5)	30.91
PLLA/SiO ₂ (90/10)	30.86
PLLA/SiO ₂ (85/15)	29.41
PLLA/SiO ₂ /PEG (90/10/3)	30.88
PLLA/SiO ₂ /PEG (90/10/5)	30.96
PLLA/SiO ₂ /PEG (90/10/8)	33.64
PLLA/SiO ₂ /PEG (90/10/10)	30.60

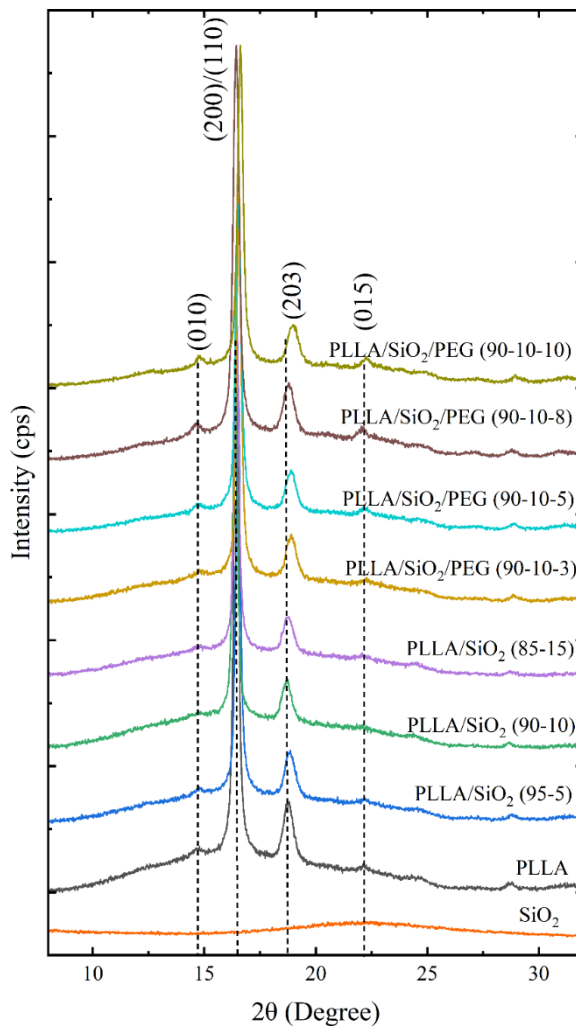


Figure 17. XRD patterns of PLLA, PLLA/SiO₂ and PLLA/SiO₂/PEG composites.

6.10 Gas Permeation Measurements

The use of fillers to improve the gas permeability in PLLA has been well documented (104–106). Table 10 presents the results obtained by the variable pressure (constant volume) method. In general, the permeability of the composites to O₂, N₂, CO₂, and CH₄ decrease as the crystallinity of the samples increase. The increase in the crystallinity implies the reduction of amorphous zones in the polymer; in this way, there is a decrease in free volume (105). PLLA/SiO₂ with 5 and 10 wt% composites exhibit an improvement in PLLA's barrier character for O₂ and CO₂ while increasing the permeability for H₂ and CH₄. This behavior explains that lots of micro pores and defects in the film can be sealed by SiO₂. The Si-O bond in SiO₂ exhibits different adsorption and release rates to different gases (107); due to the saturation of SiO₂ and Si-O bonds on the

surface of the polymeric matrix, the molecules of O₂ and CO₂ can not through the film of composites exhibiting lower values of permeability. As was expected, the increase of silica content increases free volume in the composite; consequently, the permeability decreases for all the gases. According to the values obtained for selectivity, higher values were achieved with 10 wt% of silica. However, these values can improve by changing some factors, such as temperature. It was reported that gas permeability increased with temperature, most likely due to gas molecules having more speed and momentum at higher temperatures, leading to enhanced gas permeability (106).

On the other hand, the results obtained for PLLA/SiO₂/PEG composites show a decrease in permeability for all the gases in comparison with neat PLLA, even 38% for O₂. The increase of PEG increases the dispersion of SiO₂ particles into the polymeric matrix, decreasing the mass transfer of molecules throughout the composites due to the decrease of free volume molecules will have to cross to permeate the material (96). Therefore, this result can be explained considering the arrangement structure of matrix/filler and plasticizer, making the end material with a high barrier character. Even though permeability decreases significantly for all gases, there is still a difference between O₂, and CO₂, in comparison with H₂ and CH₄. As explained above, Si-O bonds lower the permeability for O₂ and CO₂ because of the oxygen competition on the membrane surface (108). According to the selective values, there was a general decrease due to the lower gas permeability.

Table 10. Permeability of PLLA, PLLA/SiO₂, and PLLA/SiO₂/PEG composites at O₂, CO₂, H₂, and CH₄.

Sample	Permeability				Selectivity			
	O ₂	CO ₂	H ₂	CH ₄	H ₂ /O ₂	CH ₄ /CO ₂	H ₂ /CO ₂	H ₂ /CH ₄
	<i>Barrer (cm³ · cm · cm⁻² · s⁻¹ · cmHg⁻¹)</i>				<i>Barrer (cm³ · cm · cm⁻² · s⁻¹ · cmHg⁻¹)</i>			
PLA	9.36	7.49	5.56	6.53	1.68	1.15	1.35	1.17
PLA/SiO ₂ (95/5)	7.30	6.98	9.04	9.07	1.24	1.30	1.30	1.00
PLA/SiO ₂ (90/10)	6.34	6.73	10.09	8.17	1.59	1.21	1.50	1.24
PLA/SiO ₂ (85/15)	6.46	4.98	7.26	5.61	1.12	1.13	1.46	1.29
PLA/SiO ₂ /PEG (90/10/3)	4.45	4.69	5.84	5.60	1.31	1.19	1.25	1.04
PLA/SiO ₂ /PEG (90/10/5)	4.41	4.60	6.02	4.01	1.37	1.15	1.31	1.50
PLA/SiO ₂ /PEG (90/10/8)	4.80	4.98	6.10	6.11	1.27	1.23	1.22	1.00
PLA/SiO ₂ /PEG (90/10/10)	3.56	3.76	4.02	5.48	1.13	1.46	1.07	1.36

7. Conclusions

The PLLA/PEG and PLLA/SiO₂/PEG composites were successfully prepared using melt extrusion. Morphological analyses show no agglomerations but good interaction between the particle and the polymeric matrix. Due to the high miscibility of the two polymers and quantities of hydroxyl groups, adding PEG to the composite increases the SiO₂ distribution and smooths the PLLA surface.

Non-isothermal analysis shows that incorporating SiO₂ at higher concentrations increasing T_g and T_{cc} hindering the PLLA crystallization also confirmed by XRD analysis. Isothermal crystallization analysis shows that the Avrami exponent n for neat PLLA and PLLA/SiO₂ values is between 3.02-4.21, more oriented to higher values near 4, which implies sporadic tridimensional nucleation. Lauritzen-Hoffman's parameters confirm that silica particles difficult the crystallization of PLLA at those concentrations. The thermal stability of the composites increases because of the presence of non-fusible particles. SiO₂ addition to the polymer matrix increases the system's viscosity, most likely due to the disruption of the flow lines and the restriction of polymer chain mobility. Incorporating SiO₂ (10%) into the PLLA matrix improves tensile modulus by 26% while exhibiting a slight decrease of 2.4% in tensile strength. Compared with the composites with 5 and 15 wt%, the composite with 10% shows optimum mechanical performance for these composites. According to the permeability test results, PLLA/SiO₂ composites with 5 and 10 wt% show an improvement in PLLA's barrier character for O₂ and CO₂ while increasing permeability for H₂ and CH₄. Due to the saturation of SiO₂ and Si-O bonds on the surface of the polymeric matrix and the increase in crystallinity, the molecules of O₂ and CO₂ are impeded in the film composite.

For composites with PEG as plasticizer, non-isothermal analysis reveals that adding PEG into the PLLA/SiO₂ (90/10) composite reduces the T_g and T_{cc} , primarily due to plasticizing effect of the PEG and increase in the chain mobility. The highest content of PEG increases the crystallinity percentage confirmed by DSC and XRD analysis related to a higher capacity to generate α -crystalline structures decreasing T_{cc} . The Avrami exponent n for PLLA/SiO₂/PEG composites is between 2.98-3.60 showing instantaneous nucleated spherulites. By Lauritzen-Hoffman's parameters were confirm for all the PLLA/SiO₂/PEG composites, adding PEG improved polymer chain mobility and accelerated crystallization by lowering the energy required for the chain folding process.

All the rheological properties measured decreased due to diluting effect of the plasticizer that decreased viscosity and enhanced fluidity. PEG within PLLA/SiO₂ (90/10) improves the ductility of the composite while reducing its tensile strength and tensile modulus. The composite with higher content of PEG exhibited optimum elongation at the break with an increase to the tune of 26% as compared with PLLA/SiO₂ (90/10). For all gases the permeability decreases as increased PEG, causing SiO₂ particles to spread more fairly within the polymeric matrix, reducing the free volume molecules must pass through to transfer mass through composites.

8. References

1. Madhavan Nampoothiri K, Nair NR, John RP. An overview of the recent developments in polylactide (PLA) research. *Bioresour Technol* [Internet]. 2010;101(22):8493–501. Available from: <http://dx.doi.org/10.1016/j.biortech.2010.05.092>
2. Lunt J. Large-scale production, properties and commercial applications of poly lactic acid polymers. *Polym Degrad Stab*. 1998;59(1–3):145–52.
3. Auras R, Harte B, Selke S. An overview of polylactides as packaging materials. *Macromol Biosci*. 2004;4(9):835–64.
4. He Y, Fan Z, Hu Y, Wu T, Wei J, Li S. DSC analysis of isothermal melt-crystallization, glass transition and melting behavior of poly(l-lactide) with different molecular weights. *Eur Polym J*. 2007;43(10):4431–9.
5. Drumright RE, Gruber PR, Henton DE. Polylactic acid technology. *Adv Mater*. 2000;12(23):1841–6.
6. Garlotta D. A literature review of poly(lactic acid). *J Polym Environ*. 2001;9(2):63–84.
7. Stefaniak K, Masek A. Green copolymers based on poly(Lactic acid)—short review. *Materials (Basel)*. 2021;14(18).
8. Lai WC, Liao W Bin, Lin TT. The effect of end groups of PEG on the crystallization behaviors of binary crystalline polymer blends PEG/PLLA. *Polymer (Guildf)*. 2004;45(9):3073–80.
9. Wypych G. PLA poly(lactic acid). In: *Handbook of Polymers*. Elsevier; 2012. p. 436–40.
10. Díez-Rodríguez TM, Blázquez-Blázquez E, Martínez JC, Pérez E, Cerrada ML. Composites of a PLA with SBA-15 mesoporous silica: Polymorphism and properties after isothermal cold crystallization. Vol. 241, *Polymer*. 2022.
11. Buwalda SJ, Dijkstra PJ, Feijen J. Poly(ethylene glycol)-poly(L-lactide) star block copolymer hydrogels crosslinked by metal-ligand coordination. *J Polym Sci Part A Polym Chem*. 2012;50(9):1783–91.
12. Hasanuddin NI, Mokhtar WNAW, Othaman R, Anuar FH. Poly(lactic acid)-poly(ethylene glycol)/Magnesium Silicate Membrane for Methylene Blue Removal: Adsorption Behavior, Mechanism, Ionic Strength and Reusability Studies. *Membranes (Basel)*. 2022;12(2).
13. Long H, Wu Z, Dong Q, Shen Y, Zhou W, Luo Y, et al. Effect of polyethylene glycol on mechanical properties of bamboo fiber-reinforced polylactic acid composites. *J Appl Polym Sci*. 2019;136(26):3–10.
14. Praprudivongs C, Apichartsitporn M, Wongpreedee T. Effect of Commercial SiO₂ and SiO₂ from rice husk ash loading on biodegradation of Poly (lactic acid) and crosslinked Poly (lactic acid) . *IOP Conf Ser Mater Sci Eng*. 2017;244:012007.
15. Athanasoulia IG, Tarantili PA. Preparation and characterization of polyethylene

- glycol/poly(L-lactic acid) blends. *Pure Appl Chem*. 2017;89(1):141–52.
16. Zubir NHM, Sam ST, Zulkepli NN, Omar MF. The effect of rice straw particulate loading and polyethylene glycol as plasticizer on the properties of polylactic acid/polyhydroxybutyrate-valerate blends. *Polym Bull*. 2018;75(1):61–76.
 17. Rahman MA, De Santis D, Spagnoli G, Ramorino G, Penco M, Phuong VT, et al. Biocomposites based on lignin and plasticized poly(L -lactic acid). *J Appl Polym Sci*. 2013;129(1):202–14.
 18. Murariu M, Dubois P. PLA composites : From production to properties ☆. *Adv Drug Deliv Rev* [Internet]. 2016;107:17–46. Available from: <http://dx.doi.org/10.1016/j.addr.2016.04.003>
 19. Desai NP, Hubbell JA. Solution technique to incorporate polyethylene oxide and other water-soluble polymers into surfaces of polymeric biomaterials. *Biomaterials*. 1991;12(2):144–53.
 20. Jacobsen S, Fritz H. Plasticizing polylactide—the effect of different plasticizers on the mechanical properties. *Polym Eng Sci*. 1999;39(7):1303–10.
 21. Sheth M, Kumar RA, Dave V. Biodegradable Polymer Blends of Poly (lactic acid) and Poly (ethylene glycol) PL. 2008;1495–505.
 22. Yiga VA, Pagel S, Lubwama M, Epple S, Olupot PW, Bonten C. Development of fiber-reinforced polypropylene with NaOH pretreated rice and coffee husks as fillers: Mechanical and thermal properties. *J Thermoplast Compos Mater*. 2020;33(9):1269–91.
 23. Chougan M, Ghaffar SH, Al-Kheetan MJ, Gecevicius M. Wheat straw pre-treatments using eco-friendly strategies for enhancing the tensile properties of bio-based polylactic acid composites. *Ind Crops Prod* [Internet]. 2020;155(August 2020):112836. Available from: <https://doi.org/10.1016/j.indcrop.2020.112836>
 24. Hernández-Olivares F, Elizabeth Medina-Alvarado R, Burneo-Valdivieso XE, Rodrigo Zúñiga-Suárez A. Short sugarcane bagasse fibers cementitious composites for building construction. *Constr Build Mater*. 2020;247:8–10.
 25. Yalçın N, Sevinç V. Studies on silica obtained from rice husk. *Ceram Int*. 2001;27(2):219–24.
 26. Battezzatore D, Bocchini S, Alongi J, Frache A. Rice husk as bio-source of silica: Preparation and characterization of PLA-silica bio-composites. *RSC Adv*. 2014;4(97):54703–12.
 27. Soltani N, Bahrami A, Pech-Canul MI, González LA. Review on the physicochemical treatments of rice husk for production of advanced materials. *Chem Eng J* [Internet]. 2015;264:899–935. Available from: <http://dx.doi.org/10.1016/j.cej.2014.11.056>
 28. AYDIN B, GEYİKÇİ F. Effect of Silica Obtained From Rice Husk on the Structural and Thermal Properties of Polylactic Acid/Polyethylene Glycol Films. *Mugla J Sci Technol*. 2019;91–6.
 29. Imam MA, Jeelani S, Rangari VK. Thermal decomposition and mechanical characterization of poly (lactic acid) and potato starch blend reinforced with

- biowaste SiO₂. *J Compos Mater.* 2019;53(16):2315–34.
30. Ahmed W, Siraj S, Al-Marzouqi AH. 3d printing pla waste to produce ceramic based particulate reinforced composite using abundant silica-sand: Mechanical properties characterization. *Polymers (Basel).* 2020;12(11):1–19.
 31. Opaprakasit P, Boonpa S, Jaikaew N, Petchsuk A, Tangboriboonrat P. Preparation of surface-modified silica particles from rice husk ash and its composites with degradable polylactic acid. *Macromol Symp.* 2015;354(1):48–54.
 32. Nofar M, Sacligil D, Carreau PJ, Kamal MR, Heuzey M. International Journal of Biological Macromolecules Poly (lactic acid) blends : Processing , properties and applications. *Int J Biol Macromol [Internet].* 2019;125:307–60. Available from: <https://doi.org/10.1016/j.ijbiomac.2018.12.002>
 33. Murariu M, Dechief A, Ramy-ratiarison R, Paint Y, Raquez J, Dubois P, et al. Recent advances in production of poly (lactic acid) (PLA) nanocomposites : a versatile method to tune crystallization properties of PLA Recent advances in production of poly (lactic acid) (PLA) nanocomposites : a versatile method to tune crystallization properties of PLA. 2015;0324.
 34. Liu H, Zhang J. Research Progress in Toughening Modification of Poly (lactic acid). 2011;1051–83.
 35. Bourbigot S. Flame retardancy of polylactide : an overview. 2020;1413–22.
 36. Fu Y, Liu L, Zhang J. through Novel Interface Engineering for Improved Conductive. 2014;
 37. Huang Y, Wang T, Zhao X, Wang X, Zhou L, Yang Y, et al. Poly (lactic acid) / graphene oxide – ZnO nanocomposite films with good mechanical , dynamic mechanical , anti-UV and antibacterial properties. 2014;(July).
 38. Huang TC, Yeh JM, Yang JC. Effect of silica size on the thermal, mechanical and biodegradable properties of polylactide/silica composite material prepared by melt blending. *Adv Mater Res.* 2010;123–125:1215–8.
 39. Mohapatra AK, Mohanty S, Nayak SK. Effect of PEG on PLA/PEG Blend and Its Nanocomposites: A Study of Thermo-Mechanical and Morphological Characterization. *Polym Polym Compos.* 2013;2–11.
 40. Wang B, Hina K, Zou H, Zuo D, Yi C. Thermal , Crystallization , Mechanical and Decomposition Properties of Poly (lactic acid) Plasticized With Poly (ethylene glycol). 2018;
 41. Liang FLJ, Bo SZ. Tensile Properties of Polylactide / Poly (ethylene glycol) Blends. *J Polym Environ [Internet].* 2015;407–15. Available from: <http://dx.doi.org/10.1007/s10924-015-0718-7>
 42. Aws Z, Ghaleb A, Jaafar M, Rashid AA. Fabrication Methods of Carbon-Based Rubber Nanocomposites and Their Applications [Internet]. *Carbon-Based Nanofillers and Their Rubber Nanocomposites.* Elsevier Inc.; 2019. 49–64 p. Available from: <http://dx.doi.org/10.1016/B978-0-12-817342-8.00003-2>
 43. Gajjar CR, Stallrich JW, Pasquinelli MA, King MW. Process – Property Relationships for Melt-Spun Poly (lactic acid) Yarn. 2021;

44. Vouyiouka SN, Papaspyrides CD, Technical N. Mechanistic Aspects of Solid-State Polycondensation [Internet]. Vol. 4, Polymer Science:A Comprehensive Reference. Elsevier B.V.; 2012. 857–874 p. Available from: <http://dx.doi.org/10.1016/B978-0-444-53349-4.00126-6>
45. Cai J, Liu M, Wang L, Yao K, Li S, Xiong H. Isothermal crystallization kinetics of thermoplastic starch / poly (lactic acid) composites. Carbohydr Polym [Internet]. 2011;86(2):941–7. Available from: <http://dx.doi.org/10.1016/j.carbpol.2011.05.044>
46. Kang T. Isothermal Crystallization Study for Quality Assurance.
47. Lorenzo AT, Arnal ML, Albuerne J, Müller AJ. DSC isothermal polymer crystallization kinetics measurements and the use of the Avrami equation to fit the data: Guidelines to avoid common problems. Polym Test. 2007;26(2):222–31.
48. Avrami M. Granulation, phase change, and microstructure kinetics of phase change. III. J Chem Phys. 1941;9(2):177–84.
49. You W, Duan B, Wang M, Lam W. Isothermal and Non-isothermal Crystallization Kinetics of Poly(L-Lactide)/Carbonated Hydroxyapatite Nanocomposite Microspheres. Adv Divers Ind Appl Nanocomposites. 2011;(February).
50. Hoffman JD. Regime III crystallization in melt-crystallized polymers: The variable cluster model of chain folding. Polymer (Guildf). 1983;24(1):3–26.
51. Vasanthakumari R, Pennings AJ. Crystallization kinetics of poly(l-lactic acid). Polymer (Guildf). 1983;24(2):175–8.
52. Pyda M, Bopp RC, Wunderlich B. Heat capacity of poly(lactic acid). J Chem Thermodyn. 2004;36(9):731–42.
53. Di Lorenzo ML. Determination of spherulite growth rates of poly(L-lactic acid) using combined isothermal and non-isothermal procedures. Polymer (Guildf). 2001;42(23):9441–6.
54. Wu D, Wu L, Wu L, Xu B, Zhang Y, Zhang M. Nonisothermal Cold Crystallization Behavior and Kinetics of Polylactide/Clay Nanocomposites. 2007;1100–13.
55. Miyata T, Masuko T. Crystallization behavior of poly(L-lactide). Elsevier. 1997;(5515–5521):745–8.
56. Patki R, Mezghani K, Phillips PJ. Crystallization Kinetics of Polymers. Phys Prop Polym Handb. 2007;625–40.
57. Jiu HCJ, Sugahara T. Using the Friedman method to study the thermal degradation kinetics of photonicallly cured electrically conductive adhesives. 2014;
58. Saeidlou S, Huneault MA, Li H, Park CB. Poly(lactic acid) crystallization. Prog Polym Sci [Internet]. 2012;37(12):1657–77. Available from: <http://dx.doi.org/10.1016/j.progpolymsci.2012.07.005>
59. Chen X, Rodrigue D, Kaliaguine S. Diamino-organosilicone APTMDS: A new cross-linking agent for polyimides membranes. Sep Purif Technol [Internet]. 2012;86:221–33. Available from: <http://dx.doi.org/10.1016/j.seppur.2011.11.008>
60. Müller AJ, Ávila M, Saenz G, Salazar J. Crystallization of PLA-based Materials.

- In: Poly(lactic acid) Science and Technology: Processing. Royal Society of Chemistry; 2014. p. 66–100.
61. Mohapatra AK, Mohanty S. Properties and characterization of biodegradable poly (lactic acid) (PLA)/ poly (ethylene glycol) (PEG) and PLA / PEG / organoclay : A study of crystallization kinetics , rheology , and compostability. 2016;
 62. Li Y, Li X, Xiang F, Huang T, Wang Y, Wu J, et al. Crystallization, rheological, and mechanical properties of PLLA/PEG blend with multiwalled carbon nanotubes. *Polym Adv Technol.* 2011;22(12):1959–70.
 63. Nagarajan V, Mohanty AK, Misra M. Crystallization behavior and morphology of polylactic acid (PLA) with aromatic sulfonate derivative. *J Appl Polym Sci.* 2016;133(28):1–11.
 64. Michell R, Müller AJ, Boschetti-de-fierro A, Fierro D, Lison V, Raquez J, et al. Novel poly (ester-urethane) s based on polylactide : From reactive extrusion to crystallization and thermal properties. *Polymer (Guildf)* [Internet]. 2012;53(25):5657–65. Available from: <http://dx.doi.org/10.1016/j.polymer.2012.10.021>
 65. Yasuniwa M, Tsubakihara S, Sugimoto Y, Nakafuku C. Thermal analysis of the double-melting behavior of poly(L-lactic acid). *J Polym Sci Part B Polym Phys.* 2004;42(1):25–32.
 66. Tarani E, Pušnik Črešnar K, Zemljič LF, Chrissafis K, Papageorgiou GZ, Lambropoulou D, et al. Cold crystallization kinetics and thermal degradation of pla composites with metal oxide nanofillers. *Appl Sci.* 2021;11(7).
 67. Tábi T, Sajó IE, Szabó F, Luyt AS, Kovács JG. Crystalline structure of annealed polylactic acid and its relation to processing. *Express Polym Lett.* 2010;4(10):659–68.
 68. Park B, Song JC, Park DH, Yoon K. PLA / Chain-Extended PEG Blends with Improved Ductility. 2011;
 69. Saravana S, Bheemaneni G, Kandaswamy R. ScienceDirect Effect of Polyethylene glycol on Mechanical , Thermal , and Morphological Properties of Talc Reinforced Polylactic Acid Composites. *Mater Today Proc* [Internet]. 2018;5(1):1591–8. Available from: <https://doi.org/10.1016/j.matpr.2017.11.251>
 70. López C, Medina K, Ambrosio RD, Mary R, Michell RM. PLLA and cassava thermoplastic starch blends : crystalinity , mechanical properties , and UV degradation have arisen a growing interest in this material for various. 2021;16–9.
 71. Li D, Jiang Y, Lv S, Liu X, Gu J, Chen Q, et al. Preparation of plasticized poly (lactic acid) and its influence on the properties of composite materials. 2018;13(3):1–15.
 72. Wang Y, Mano JF. Influence of melting conditions on the thermal behaviour of poly(l-lactic acid). *Eur Polym J.* 2005;41(10):2335–42.
 73. Iannace S, Nicolais L. of Poly (L -lactide). 1996;911–9.
 74. Marand H, Xu J, Srinivas S. Determination of the equilibrium melting temperature of polymer crystals: Linear and nonlinear Hoffman-Weeks extrapolations. *Macromolecules.* 1998;31(23):8219–29.

75. Karimi S, Ghasemi I, Abbassi-Sourki F. A study on the crystallization kinetics of PLLA in the presence of Graphene Oxide and PEG-grafted-Graphene Oxide: Effects on the nucleation and chain mobility. *Compos Part B Eng* [Internet]. 2019;158:302–10. Available from: <https://doi.org/10.1016/j.compositesb.2018.10.004>
76. Song R, Xue R, He L, Liu Y, Xiao Q. the Structure and Properties of Chitosan / Polyethylene. *Polym Sci*. 2008;26(5):621–30.
77. Song Y, Wang D, Jiang N, Gan Z. Role of PEG Segment in Stereocomplex Crystallization for PLLA/PDLA- b -PEG- b -PDLA Blends. *ACS Sustain Chem Eng*. 2015;3(7):1492–500.
78. Nazari T, Garmabi H. Thermo-rheological and interfacial properties of polylactic acid/polyethylene glycol blends toward the melt electrospinning ability. *J Appl Polym Sci*. 2016;133(44):1–11.
79. Mandelkern L. *Crystallization of Polymers*. Cambridge University Press; 2004. 217–281 p.
80. Zhang J, Wang S, Zhao D, Zhang Y, Pang W, Zhang B, et al. Improved processability and performance of biomedical devices with poly (lactic acid)/ poly (ethylene glycol) blends. 2017;45194:1–8.
81. Succinate PH, Chrysafi I, Ainali NM. Thermal Degradation Mechanism and Decomposition Kinetic Studies of Poly (Lactic Acid) and Its Copolymers with. 2021;
82. Zou H, Yi ÆC, Wang ÆL. Thermal degradation of poly (lactic acid) measured by thermogravimetry coupled to Fourier transform infrared spectroscopy. 2009;929–35.
83. Henrique P, Cardoso M, Ferreira M, Oliveira L De, De MG, Mara R, et al. 3D Printed Parts of Polylactic Acid Reinforced with Carbon Black and Alumina Nanofillers for Tribological Applications. 2020;2000155:1–13.
84. Zhou H, Zhao M, Qu Z, Mi J, Wang X, Deng Y. Thermal and Rheological Properties of Poly (lactic acid)/ Low-Density Polyethylene Blends and Their Supercritical - CO 2 Foaming Behavior. *J Polym Environ* [Internet]. 2018;0(0):0. Available from: <http://dx.doi.org/10.1007/s10924-018-1240-5>
85. Wang R, Wang S, Zhang Y, Wan C, Ma P. Toughening Modification of PLLA/PBS Blends via In Situ Compatibilization. *Polym Eng Sci*. 2009;26–33.
86. Gao Y, Qu W, Liu Y, Hu H, Cochran E, Bai X. Agricultural residue-derived lignin as the fi ller of polylactic acid composites and the effect of lignin purity on the composite performance. 2019;47915:1–9.
87. Gong J, Tian N, Wen X, Chen X, Liu J, Jiang Z, et al. Synergistic effect of fumed silica with Ni 2 O 3 on improving fl ame retardancy of poly (lactic acid). *Polym Degrad Stab* [Internet]. 2014;104:18–27. Available from: <http://dx.doi.org/10.1016/j.polymdegradstab.2014.03.030>
88. Delgado PA, Brutman JP, Masica K, Molde J, Wood B, Hillmyer MA. High surface area carbon black (BP-2000) as a reinforcing agent for poly[(2)-lactide]. 2016;

89. Liu Y, Shao J, Sun J, Bian X, Feng L, Xiang S, et al. Improved mechanical and thermal properties of PLLA by solvent blending with PDLA-b-PEG-b-PDLA. *Polym Degrad Stab* [Internet]. 2014;101(1):10–7. Available from: <http://dx.doi.org/10.1016/j.polymdegradstab.2014.01.023>
90. Zhao P, Liu Z, Wang X, Pan YT, Kuehnert I, Gehde M, et al. Renewable vanillin based flame retardant for poly(lactic acid): A way to enhance flame retardancy and toughness simultaneously. *RSC Adv*. 2018;8(73):42189–99.
91. Tao Y, Liu M, Han W, Li P. Waste office paper filled polylactic acid composite filaments for 3D printing. *Compos Part B* [Internet]. 2021;221(May):108998. Available from: <https://doi.org/10.1016/j.compositesb.2021.108998>
92. Jia Z, Zhang K, Tan J, Han C, Dong L, Yang Y. Crystallization Behavior and Mechanical Properties of Crosslinked Plasticized Poly(L-lactic acid). *Appl Polym Sci*. 2008;1531–9.
93. Dekkers MEJ, Heikens D. The effect of interfacial adhesion on the tensile behavior of polystyrene–glass-bead composite.pdf. *J Appl Polym Sci*. 1983;28(12):3809–15.
94. Mackay ME. Principles of polymer engineering rheology. Vol. 39, *Journal of Non-Newtonian Fluid Mechanics*. 1991. p. 211.
95. Zhang Q, Mochalin VN, Neitzel I, Hazeli K, Niu J, Kontsos A, et al. Mechanical properties and biomineralization of multifunctional nanodiamond-PLLA composites for bone tissue engineering. *Biomaterials* [Internet]. 2012;33(20):5067–75. Available from: <http://dx.doi.org/10.1016/j.biomaterials.2012.03.063>
96. Alberton J, Martelli SM, Fakhouri FM, Soldi V. Mechanical and moisture barrier properties of titanium dioxide nanoparticles and halloysite nanotubes reinforced polylactic acid (PLA). *IOP Conf Ser Mater Sci Eng*. 2014;64(1).
97. Hong Z, Zhang P, He C, Qiu X, Liu A, Chen L, et al. Nano-composite of poly(L-lactide) and surface grafted hydroxyapatite: Mechanical properties and biocompatibility. *Biomaterials*. 2005;26(32):6296–304.
98. Zhang Q, Mochalin VN, Neitzel I, Knoke IY, Han J, Klug CA, et al. Fluorescent PLLA-nanodiamond composites for bone tissue engineering. *Biomaterials* [Internet]. 2011;32(1):87–94. Available from: <http://dx.doi.org/10.1016/j.biomaterials.2010.08.090>
99. Daia X, Yu C, Shia X, Wang X. Non-isothermal crystallization kinetics, thermal degradation behavior and mechanical properties of poly(lactic acid)/MOF composites prepared by melt-blending methods. 2016;
100. Hara S, Watanabe S, Takahashi K, Shimizu S, Ikake H. Preparation of Crystallites for Oriented Poly (Lactic Acid) Films Using a Casting Method under a Magnetic Field. 2018;
101. Huang S, Li H, Jiang S, Chen X, An L. Crystal structure and morphology influenced by shear effect of poly(l-lactide) and its melting behavior revealed by WAXD, DSC and in-situ POM. *Polymer (Guildf)* [Internet]. 2011;52(15):3478–87. Available from: <http://dx.doi.org/10.1016/j.polymer.2011.05.044>

102. Xu H, Zhong G, Fu Q, Lei J, Jiang W, Hsiao BS, et al. Formation of Shish-Kebabs in Injection-Molded Poly(. 2012;
103. You J, Yu W, Zhou C. Accelerated crystallization of poly(lactic acid): Synergistic effect of poly(ethylene glycol), dibenzylidene sorbitol, and long-chain branching. *Ind Eng Chem Res.* 2014;53(3):1097–107.
104. Kathuria A, Al-Ghamdi S, Abiad MG, Auras R. The influence of Cu₃(BTC)₂ metal organic framework on the permeability and perm-selectivity of PLLA-MOF mixed matrix membranes. *J Appl Polym Sci.* 2015;132(46):1–10.
105. Lizundia E, Vilas JL, Sangroniz A, Etxeberria A. Light and gas barrier properties of PLLA/metallic nanoparticles composite films. *Eur Polym J [Internet].* 2017;91:10–20. Available from: <http://dx.doi.org/10.1016/j.eurpolymj.2017.03.043>
106. Dong T, Song S, Liang M, Wang Y, Qi X, Zhang Y, et al. Gas Permeability and Permselectivity of Poly(L-Lactic Acid)/SiO_x Film and Its Application in Equilibrium-Modified Atmosphere Packaging for Chilled Meat. *J Food Sci.* 2017;82(1):97–107.
107. Yampolskii Y. Polymeric gas separation membranes. *Macromolecules.* 2012;45(8):3298–311.
108. Dury-Brun C, Chalier P, Desobry S, Voilley A. Multiple mass transfers of small volatile molecules through flexible food packaging. *Food Rev Int.* 2007;23(3):199–255.